

A DIRAC-HARTREE-BOGOLIUBOV APPROXIMATION FOR FINITE NUCLEI

B.V. Carlson

*Departamento de Física,
Instituto Tecnológico da Aeronáutica,
Centro Técnico Aeroespacial, 12228-900 São José dos Campos,
São Paulo, Brazil*

D. Hirata*

*Japan Synchrotron Radiation Research Institute (JASRI) - SPring-8,
Kamigori, Hyogo, 678-12, Japan
(October 28, 2018)*

Abstract

We develop a complete Dirac-Hartree-Fock-Bogoliubov approximation to the ground state wave function and energy of finite nuclei. We apply it to spin-zero proton-proton and neutron-neutron pairing within the Dirac-Hartree-Bogoliubov approximation (we neglect the Fock term), using a zero-range approximation to the relativistic pairing tensor. We study the effects of the pairing on the properties of the even-even nuclei of the isotopic chains of Ca, Ni and Sn (spherical) and Kr and Sr (deformed), as well as the $N=28$ isotonic chain, and compare our results with experimental data and with other recent calculations.

PACS number(s): 21.65.+f, 72.40.F, 21.60.J

Typeset using REVTeX

*present address: GANIL, BP5027, Bd Becquerel, 14076 Caen Cedex 5, France

I. INTRODUCTION

The advances made at radioactive nuclear beam facilities provide us with an increasing amount of information on nuclei far away from the stability line. We now have access to experimental measurements of the masses, radii and deformations of unstable nuclei in a wider region of the nuclear chart than ever before. Studies of exotic nuclei have revealed new features, such as neutron halos [1] and neutron skins [2,3] and bring new perspectives to nuclear physics [4]. Planned facilities around the world plan to study unstable nuclei up to the r-process region or even beyond. This will enable us to investigate where and how exotic phenomena of nuclear structure appear in the region far from the stability line [5,6].

In recent years relativistic many-body theories have been applied to nuclei and nuclear matter with remarkable success [7–9]. The relativistic Brueckner-Hartree-Fock (RBHF) theory has been shown capable of reproducing the saturation properties of nuclear matter using interaction parameters that describe the two-nucleon bound state and scattering [10]. Its phenomenological version, the relativistic mean field model (RMF), has been successfully applied to the description of many of the ground-state properties of stable and unstable nuclei [11–24] and has been shown capable of simultaneously reproducing the properties of stable and unstable nuclei over a wide mass range of the periodic table [25].

The relativistic mean field approach has also been applied to describe the structure of very exotic nuclei. In these calculations, the pairing interaction has been neglected or simply treated by a nonrelativistic BCS type of approximation [25,26]. For nuclei on or near the stability line, the BCS approach provides a reasonably good description of pairing properties. However, for drip-line nuclei, the Fermi level is close to the continuum and the coupling between bound and continuum states should be taken into account explicitly. The pairing correlations and the mean fields should be calculated simultaneously in order to obtain an accurate description of the ground state properties of drip-line nuclei.

A more precise relativistic description of pairing correlations, a Dirac-Hartree-Fock-Bogoliubov (DHFB) approximation, was developed some time ago [27] and, more recently, applied to nuclear matter calculations [28–31]. The first calculations in nuclear matter furnished pairing gaps much larger than those obtained in nonrelativistic calculations using realistic interactions. [28] The results suggested that the meson-exchange interactions adjusted to describe nuclear matter saturation might not be adequate for the particle-particle pairing channel. However, these calculations did not perform a complete self-consistent DHFB calculation. Rather, they combined a relativistic Hartree mean field calculation with a nonrelativistic calculation of the pairing field using the nonrelativistic reduction of the meson-exchange potential. Self-consistent calculations including the full Dirac structure of the self-energy and pairing fields resulted in more reasonable values for the pairing gap. [29,30] Yet these DHFB calculations, using various sets of meson-exchange parameters that furnish similar good descriptions of nuclear saturation, still resulted in values of the pairing gap that were not consistent with nonrelativistic calculations nor consistent among themselves. In Ref. [31], these discrepancies were resolved by associating the pairing gap of each set of meson-exchange parameters with the set's description of low-energy two-nucleon scattering in the 1S_0 channel. When each of the parameter sets was supplemented with a momentum cutoff, so that they each described the two-nucleon 1S_0 virtual state correctly, they all provided consistent values for the pairing gap that very close to the nonrelativistic

ones, at low densities. Thus, the conclusion of Ref. [28] was found to be correct after all. The meson-exchange interactions adjusted to describe nuclear matter saturation are indeed inadequate for the pairing channel, when they do not describe the two-nucleon 1S_0 channel well. In the case of nuclear matter, however, we have found that this inadequacy can be easily remedied.

Even after the different sets of meson-exchange parameters have been augmented so as to describe the two-nucleon 1S_0 channel, they still differ slightly among themselves at densities greater than about one-eighth of the saturation density, where mean field effects begin to play a role. Most importantly, they all differ in a consistent manner from the gap functions obtained using realistic nonrelativistic two-nucleon interactions. The relativistic pairing gap consistently falls to zero at lower density (by about one-half) of that for which it disappears in nonrelativistic calculations. Much as the Dirac structure of the nuclear mean field weakens the effective interaction as the density increases, leading to saturation, so the Dirac structure of the pairing field weakens the effective pairing interaction with density, leading to the suppression of the pairing field relative to the nonrelativistic one. An estimate of the relativistic effects on quasi-deuteron pairing shows that the same effects also suppress quasi-deuteron pairing at the saturation density [32]. We thus expect a density-dependent suppression of the pairing field to be a general feature when we take the Dirac structure of the field into account.

The relativistic Hartree mean field + nonrelativistic pairing field approximation of Ref. [28] can and has been extended to finite nuclei. This hybrid relativistic Hartree-Bogoliubov (RHB) approximation, using a non-relativistic finite-range Gogny interaction in the pairing channel, has been applied extensively, and quite successfully, to the calculation of the ground state properties of spherical [33–41] and deformed nuclei [42]. We would expect reasonable results from such a model as long as the mean field is well described by the meson exchange interaction and the 1S_0 two-nucleon channel is well described by the effective pairing interaction. This is indeed the case in the references cited here. However, we might expect its pairing interaction to be less reliable than a meson-exchange one when extrapolated far beyond the stability valley, the condition for which its parameters have been adjusted.

Aside from simply being more pleasing aesthetically, we are motivated to retain the Dirac structure of the pairing interaction in our calculations by the success of our studies of 1S_0 pairing in nuclear matter and by their differences from the nonrelativistic results. The success of our nuclear matter calculations lead us to believe that a good description of nuclei can be obtained using a Dirac pairing interaction based on a meson-exchange one. Such a description would be of general interest, since the Dirac structure of a meson-exchange interaction could be extended beyond the valley of stability with better reliability than could a nonrelativistic interaction. A nonrelativistic effective interaction must incorporate the density dependence furnished by the Dirac structure of a meson-exchange interaction into its effective parameters. This density dependence changes as we consider nuclei further and further from the stability valley, thus limiting the range of application of a effective interaction adjusted to describe the conditions in the valley.

The differences between our results and nonrelativistic ones in nuclear matter suggest that interesting effects of the Dirac structure of the pairing interaction might appear even in nuclei within the stability valley. The suppression of pairing in the saturated interior region,

in DHFB calculations, similar to that observed in nuclear matter, would result in greater localization of the pairing field on the nuclear surface than is the case in nonrelativistic or RHB calculations. This, in turn, would tend to make the nucleus more rigid and tend to diminish its deformation. We then would expect to observe a smaller pairing field in DHB calculations that furnish the same deformation as nonrelativistic or RHB ones, or a smaller deformation in DHB calculations that furnish the same value of the pairing field as nonrelativistic or RHB ones.

Here we present a fully relativistic Dirac-Hartree-Bogoliubov (DHB) approximation for axially deformed nuclei. We use a direct extension of the DHFB approximation developed in Ref. [29]. We neglect the exchange term in the self-energy but retain the Dirac structure of the pairing interaction and pairing field. The neglect of the exchange term seems a reasonable approximation here, as we restrict our calculations to the exchange of σ , ρ and ω mesons, for which the exchange effects can be fairly well accommodated by adjustments in the coupling constants. The characteristics of the pairing field and of its Dirac structure will form the center of our study. Our goal is to extend our successful DHFB description of nuclear matter to a DHB description of finite nuclei.

We use a local (zero-range) approximation to the meson-exchange interaction in the pairing channel. A zero-range approximation to the pairing interaction can be justified by an analysis of the length scales in a typical DHB calculation. Taking oscillator wave functions as a guide, we can estimate the wavelength in one dimension of a wave function of quantum number n (in that dimension) as $\lambda_n \approx 4.4b_0/\sqrt{n}$, where b_0 is the oscillator length, $b_0 \approx A^{1/6}$ fm, and A is the mass number of the nucleus. In the fairly extreme case of the $N=16$ shell of ^{16}O , we find a wavelength of $\lambda_{16} \approx 1.75$ fm. The wavelength is larger in heavier nuclei or in lower shells. On the other hand, the range of a typical meson-exchange interaction is $r_x = \hbar c/m$, where m is the meson mass. For the lightest of the mesons that we include, the σ meson, we find a range of $r_\sigma < 0.5$ fm, substantially smaller than the wavelength λ_{16} . Even the term of longest range of the Gogny interaction has $r_2 = 1.2$ fm only. Thus we find that the interaction range is typically smaller than the length scale of the most energetic level, making the effects due to the finite range of the interaction small. This analysis has, in fact, been confirmed numerically by Meng [38], who found zero-range and finite-range Gogny RHB calculations to yield almost identical results.

In Section I of the following, we derive the self-consistency equations for the self-energy and pairing fields. In Section II, we discuss the properties of static solutions to the equations and, in Section III, reduce these to the form in which we use them. In Section IV, we briefly describe the numerical method used in the calculations and, in Section V, we discuss the results of the calculations. We summarize and conclude in Section VI.

II. THE MEAN FIELD EQUATIONS FOR Σ AND Δ

In this section we present the Lagrangian of the model and the covariant equations for the self-energy and pairing mean fields, Σ and Δ .

We designate by $\psi(x)$, $\sigma(x)$, $\omega^\mu(x)$, $\vec{\rho}^\mu(x)$, and $A^\mu(x)$, the field operators at the point x associated to the nucleons and mesons σ , ω , ρ , and γ respectively. The quantum numbers (J^π, T) for each meson with spin J , intrinsic parity π , and isospin T are

$$\sigma(0^+, 0), \quad \omega(1^-, 0), \quad \rho(1^-, 1), \quad \gamma(1^-, -).$$

We designate the effective meson-nucleon coupling constants by g_s , g_v and g_ρ and the respective bare masses by m_s , m_v and m_ρ . The interaction of the massless γ does not conserve isospin, coupling to the protons alone with coupling constant e . (We will ignore the interaction with the anomalous magnetic moments of the nucleons). The nucleon bare mass is M and we assume in the present model that the nucleons and mesons are point-like. We will not take the π meson into account, although its effects could be important in the exchange terms we will consider. We will assume that these effects can be described through the effective couplings of the mesons we do include. These assumptions are typical of the simplest meson-exchange models of nuclear structure.

The Lagrangian density is given by

$$\mathcal{L} = \mathcal{L}_0 + \mathcal{L}_{int},$$

where \mathcal{L}_0 is the free Lagrangian density

$$\begin{aligned} \mathcal{L}_0(x) = & \bar{\psi}(x)[i\not{\partial} - M]\psi(x) + \frac{1}{2}\partial_\mu\sigma(x)\partial^\mu\sigma(x) - U(\sigma(x)) - \frac{1}{4}F_{\mu\nu}F^{\mu\nu} \\ & - \frac{1}{4}\Omega_{\mu\nu}\Omega^{\mu\nu} + \frac{1}{2}m_v^2\omega_\mu(x)\omega^\mu(x) - \frac{1}{4}\vec{G}_{\mu\nu} \cdot \vec{G}^{\mu\nu} + \frac{1}{2}m_\rho^2\vec{\rho}_\mu(x) \cdot \vec{\rho}^\mu(x), \end{aligned} \quad (1)$$

with vector field tensors

$$\begin{aligned} F_{\mu\nu} &= \partial_\mu A_\nu - \partial_\nu A_\mu, \\ \Omega_{\mu\nu} &= \partial_\mu \omega_\nu - \partial_\nu \omega_\mu, \\ \vec{G}_{\mu\nu} &= \partial_\mu \vec{\rho}_\nu - \partial_\nu \vec{\rho}_\mu, \end{aligned}$$

and a nonlinear σ potential,

$$U(\sigma(x)) = \frac{1}{2}m_s^2\sigma(x)^2 + \frac{1}{3}g_3\sigma(x)^3 + \frac{1}{4}g_4\sigma(x)^4. \quad (2)$$

The baryon spinor $\psi(x)$ has four Dirac components for each of two isospin projections – $m_t = 1/2$ for protons and $m_t = -1/2$ for neutrons – for a total of eight components. We have included the cubic and quartic terms of the scalar field $\sigma(x)$ in the free Lagrangian density as we will only consider their contributions to the scalar mean field. For this purpose, we may formally include them in the ‘free’ scalar meson propagator, when it is convenient to do so.

We take the interaction terms in the Lagrangian density to have the simplest possible form consistent with their Lorentz and isospin structure,

$$\begin{aligned} \mathcal{L}_{int}(x) = & g_s\bar{\psi}(x)\sigma(x)\psi(x) - g_v\bar{\psi}(x)\gamma_\mu\omega^\mu(x)\psi(x) - \frac{1}{2}g_\rho\bar{\psi}(x)\gamma_\mu\vec{\tau} \cdot \vec{\rho}^\mu(x)\psi(x) \\ & - e\bar{\psi}(x)\frac{(1 + \tau_3)}{2}\gamma_\mu A^\mu(x)\psi(x). \end{aligned} \quad (3)$$

In particular, we will not consider tensor couplings of the vector mesons.

We wish to characterize the average effect of the interactions of a nucleon with the other nucleons through an effective single-particle Lagrangian, L_{eff} , given in terms of the two fields, Σ and Δ . The self-energy Σ describes the average interaction of a nucleon with the surrounding matter. The pairing field Δ and its conjugate $\bar{\Delta}$ describe, respectively, the formation and destruction of pairs during the propagation. In particular, the definition of Δ makes use of correlated pairs of time-reversed single-particle states, in agreement with the original idea of Cooper [43]. Generalizing slightly the development due to Gorkov [44], we introduce such pairs by using an extended form of the time-reversed states, which we designate by ψ_T . Designating the time reversal operator by \mathcal{T} , the usual time-reversed conjugate $\psi^{(\mathcal{T})}$ of the Dirac field operator ψ is given by [45]

$$\psi^{(\mathcal{T})}(x) = \mathcal{T}\psi(x)\mathcal{T}^{-1} = B\bar{\psi}^T(\tilde{x}) = \gamma_0 B\psi^*(\tilde{x})$$

where

$$\tilde{x} = (-t, \vec{x}), \quad B = \gamma_5 C,$$

and C is the charge conjugation operator. We define ψ_T as

$$\psi_T(x) = \tau_2 \otimes \psi^{(\mathcal{T})}(\tilde{x}) \equiv A\bar{\psi}^T(x),$$

where $A = \tau_2 \otimes B$ and τ_2 is the antisymmetric Pauli matrix, which operates here in the isospin space. Note that $A = A^T$ and $A^* = A^\dagger$. We then use the following ansatz for the effective single-particle Lagrangian

$$\int dt L_{eff} = \int d^4x d^4y \left\{ \bar{\psi}(x) [i\cancel{\partial} - M + \gamma_0\mu] \delta(x-y)\psi(y) - \bar{\psi}(x)\Sigma(x,y)\psi(y) \right. \\ \left. + \frac{1}{2}\bar{\psi}(x)\Delta(x,y)\psi_T(y) + \frac{1}{2}\overline{\psi_T}(x)\bar{\Delta}(x,y)\psi(y) \right\}, \quad (4)$$

where $\delta(x-y)$ is a four-dimensional Dirac delta function and

$$\mu = \begin{pmatrix} \mu_p & 0 \\ 0 & \mu_n \end{pmatrix} \quad (5)$$

is the isospin matrix of chemical potentials, which will be used as Lagrange multipliers to fix the average number of protons and neutrons.

The symmetries of the effective mean-field Lagrangian under transposition and Hermitian conjugation yield the following properties of the mean fields,

$$\Delta(x,y) = -A \Delta^T(x,y) A^\dagger = -A (\Delta(y,x))^T A^\dagger \quad \text{and} \quad \bar{\Delta}(x,y) = -A \bar{\Delta}^T(x,y) A^\dagger, \quad (6)$$

and

$$\Sigma(x,y) = \gamma_0 \Sigma^\dagger(x,y) \gamma_0 \quad \text{and} \quad \Delta(x,y) = \gamma_0 \bar{\Delta}^\dagger(x,y) \gamma_0. \quad (7)$$

The first of these symmetry conditions requires that the pair wave function be antisymmetric under exchange while the second guarantees real energy eigenvalues and probability conservation.

We can put the effective Lagrangian L_{eff} in a more symmetrical form by noting that

$$\begin{aligned} \int d^4x d^4y \quad \bar{\psi}(x) [(i\rlap{\not{\partial}} - M + \gamma_0\mu)\delta(x-y) - \Sigma(x,y)] \psi(y) \\ = \int d^4x d^4y \quad \bar{\psi}_T(x) [(i\rlap{\not{\partial}} + M - \gamma_0\mu)\delta(x-y) + \Sigma_T(x,y)] \psi_T(y), \end{aligned} \quad (8)$$

where

$$\Sigma_T(x,y) = A\Sigma^T(x,y)A^\dagger, \quad (9)$$

The effective Lagrangian can then be rewritten in matrix form as

$$\begin{aligned} \int dt L_{eff} = \frac{1}{2} \int d^4x d^4y \quad (\bar{\psi}(x), \bar{\psi}_T(x)) \\ \times \begin{pmatrix} (i\rlap{\not{\partial}} - M + \gamma_0\mu)\delta(x-y) - \Sigma(x,y) & \Delta(x,y) \\ \bar{\Delta}(x,y) & (i\rlap{\not{\partial}} + M - \gamma_0\mu)\delta(x-y) + \Sigma_T(x,y) \end{pmatrix} \begin{pmatrix} \psi(y) \\ \psi_T(y) \end{pmatrix}, \end{aligned} \quad (10)$$

which immediately yields the following coupled equations of motion for the fields ψ and ψ_T , which we will call the Dirac-Gorkov equation,

$$\int d^4y \begin{pmatrix} (i\rlap{\not{\partial}} - M + \gamma_0\mu)\delta(x-y) - \Sigma(x,y) & \Delta(x,y) \\ \bar{\Delta}(x,y) & (i\rlap{\not{\partial}} + M - \gamma_0\mu)\delta(x-y) + \Sigma_T(x,y) \end{pmatrix} \begin{pmatrix} \psi(y) \\ \psi_T(y) \end{pmatrix} = 0. \quad (11)$$

Defining the generalized baryon field operator as

$$\Psi(x) = \begin{pmatrix} \psi(x) \\ \psi_T(x) \end{pmatrix},$$

we obtain a generalized baryon (quasi-particle) propagator

$$S(x,y) = \begin{pmatrix} G(x,y) & F(x,y) \\ \tilde{F}(x,y) & \tilde{G}(x,y) \end{pmatrix} = -i \left\langle \begin{pmatrix} \psi(x) \\ \psi_T(x) \end{pmatrix} (\bar{\psi}(y), \bar{\psi}_T(y)) \right\rangle, \quad (12)$$

where, by $\langle \dots \rangle$, we mean the time-ordered expectation value in the interacting nuclear ground state, $\langle \tilde{0} | T(\dots) | \tilde{0} \rangle$. We assume that the state $|\tilde{0}\rangle$ contains only nucleons interacting through the exchange of virtual mesons and contains no real mesons.

We observe that $G(x,y)$ is the usual baryon propagator while $\tilde{G}(x,y)$ describes the propagation of baryons in time-reversed states. The off-diagonal terms of $S(x,y)$ describe the propagation of correlated baryons and are the relativistic generalizations of the anomalous propagators defined by Gorkov [44].

To derive the mean field equations, we first rewrite the interaction terms of the Lagrangian density, \mathcal{L}_{int} , as

$$\mathcal{L}_{int}(x) = - \sum_j \bar{\psi}(x) \Gamma_{j\alpha}(x) \phi_j^\alpha(x) \psi(x), \quad (13)$$

where the Greek letters α, β, \dots represent any indices necessary for the correct description of the meson propagation and coupling (Lorentz indices, isospin, etc.). The index j indicates

the mesons of the model: σ , ω , π , and ρ , while their respective fields and meson-nucleon couplings are designated by the $\phi_j^\alpha(x)$ and the $\Gamma_{j\alpha}(x)$.

We then rewrite the meson fields ϕ_j in terms of their sources as

$$\phi_j^\alpha(x) = \int d^4y D_j^{\alpha\beta}(x-y) \bar{\psi}(y) \Gamma_{j\beta}(y) \psi(y), \quad (14)$$

where $D_j^{\alpha\beta}(x-y)$ is the Feynman propagator of meson j . Here, we have included the non-linear σ -meson terms in the σ -meson propagator, so that they do not appear as corrections to the source term. Substituting in Eq. (13) and inserting a factor of 1/2 for reasons of symmetry, we have

$$\int dt L_{int} = -\frac{1}{2} \sum_j \int d^4x d^4y \bar{\psi}(x) \Gamma_{j\alpha}(x) \psi(x) D_j^{\alpha\beta}(x-y) \bar{\psi}(y) \Gamma_{j\beta}(y) \psi(y). \quad (15)$$

Following Gorkov [44], we then obtain the mean field contribution of this interaction term by replacing each of the possible pairs of fermion fields by its vacuum expectation value,

$$\begin{aligned} \int dt (L_{int})_{eff} = & -\frac{1}{2} \sum_j \int d^4x d^4y D_j^{\alpha\beta}(x-y) \left\{ 2\bar{\psi}(x) \Gamma_{j\alpha}(x) \psi(x) \langle \bar{\psi}(y) \Gamma_{j\beta}(y) \psi(y) \rangle \right. \\ & + 2\bar{\psi}(x) \Gamma_{j\alpha}(x) \langle \psi(x) \bar{\psi}(y) \rangle \Gamma_{j\beta}(y) \psi(y) \\ & - \bar{\psi}(x) \Gamma_{j\alpha}(x) \langle \psi(x) \psi^T(y) \rangle \Gamma_{j\beta}^T(y) \bar{\psi}^T(y) \\ & \left. - \psi^T(x) \Gamma_{j\alpha}^T(x) \langle \bar{\psi}^T(x) \bar{\psi}(y) \rangle \Gamma_{j\beta}(y) \psi(y) \right\}. \end{aligned} \quad (16)$$

where $\langle \dots \rangle$ is again the time-ordered expectation value in the interacting nuclear-matter ground state.

The first term in this expression is a Hartree one, the second a Fock exchange term while the last two, after using the definition of ψ_T to replace the transposed ψ 's, can be recognized as pairing terms. Comparing the mean field contributions to those of the effective quasi-particle Lagrangian, we can express the self-energy and pairing fields in terms of the two-fermion vacuum expectation values as

$$\begin{aligned} \Sigma(x, y) = & \delta(x-y) \sum_j \Gamma_{j\alpha}(x) \int d^4z D_j^{\alpha\beta}(x-z) \langle \bar{\psi}(z) \Gamma_{j\beta}(z) \psi(z) \rangle \\ & + \sum_j \Gamma_{j\alpha}(x) D^{\alpha\beta}(x-y) \langle \psi(x) \bar{\psi}(y) \rangle \Gamma_{j\beta}(y), \end{aligned} \quad (17)$$

and

$$\Delta(x, y) = \sum_j \Gamma_{j\alpha}(x) D_j^{\alpha\beta}(x-y) \langle \psi(x) \bar{\psi}_T(y) \rangle A \Gamma_\beta^T(y) A^\dagger, \quad (18)$$

while the equation for $\bar{\Delta}(x-y)$ can be obtained from the equation for $\Delta(x-y)$ using the Hermiticity condition of Eq. (7). These expressions become self-consistency equations when we evaluate the expectation values by using their relationship to the generalized baryon propagator, Eq. (12), which is itself a function of the mean fields. We find

$$\begin{aligned} \Sigma(x, y) = & -i\delta(x - y) \sum_j \Gamma_{j\alpha}(x) \int d^4z D_j^{\alpha\beta}(x - z) \text{Tr} \left[\Gamma_{j\beta}(z) G(z, z^+) \right] \\ & + i \sum_j \Gamma_{j\alpha}(x) D_j^{\alpha\beta}(x - y) G(x, y) \Gamma_{j\beta}(y), \end{aligned} \quad (19)$$

and

$$\Delta(x, y) = i \sum_j \Gamma_{j\alpha}(x) D_j^{\alpha\beta}(x - y) F(x, y) A \Gamma_{j\beta}^T(y) A^\dagger. \quad (20)$$

The number of protons Z and neutrons N are the expectation values of the baryon number operators, $\hat{N} = \bar{\psi}(x) \gamma_0 (1 \pm \tau_3) \psi(x) / 2$, which we rewrite in terms of the generalized baryon propagator [7], as

$$\left. \begin{array}{l} Z \\ N \end{array} \right\} = \int d^3x \left\langle \bar{\psi}(x) \gamma_0 \frac{(1 \pm \tau_3)}{2} \psi(x) \right\rangle = -i \int d^3x \text{Tr} \left[\gamma_0 \frac{(1 \pm \tau_3)}{2} G(x, x^+) \right]. \quad (21)$$

The Lagrange multipliers μ_p and μ_n , given in Eq. (5), are determined by requiring that these equations yield the desired values of Z and N .

The Hamiltonian density operator is given by the \hat{T}^{00} component of the energy-momentum tensor,

$$\hat{H} = \hat{T}^{00} = -\mathcal{L} + \frac{\partial \mathcal{L}}{\partial(\partial_t \psi)} \partial_t \psi + \sum_j \frac{\partial \mathcal{L}}{\partial(\partial_t \phi_j^\alpha)} \partial_t \phi_j^\alpha. \quad (22)$$

Neglecting the retardation terms associated with the time derivatives of the meson fields in the ground state expectation value of Eq. (22), the energy density that results can be written as

$$\begin{aligned} \mathcal{E}(x) = \langle \hat{H} \rangle = & i \text{Tr} \left[(i\vec{\gamma} \cdot \vec{\partial} - M) G(x, x^+) \right] - \frac{1}{6} g_3 \sigma(x)^3 - \frac{1}{4} g_4 \sigma(x)^4 \\ & - \frac{i}{2} \int d^4y \text{Tr} \left[\Sigma(x, y) G(y, x^+) - \Delta(x, y) \tilde{F}(y, x) \right]. \end{aligned} \quad (23)$$

The total energy is obtained by integrating this density over space.

III. PROPERTIES OF STATIC SOLUTIONS

We will develop a static, ground-state solution to the self-consistency equations. We write the temporal Fourier transform of the full HFB propagator as

$$\begin{aligned} S(\vec{x}, \vec{y}; \omega) = & \begin{pmatrix} G(\vec{x}, \vec{y}; \omega) & F(\vec{x}, \vec{y}; \omega) \\ \tilde{F}(\vec{x}, \vec{y}; \omega) & \tilde{G}(\vec{x}, \vec{y}; \omega) \end{pmatrix} = \sum_\alpha \begin{pmatrix} U_\alpha(\vec{x}) \\ V_\alpha(\vec{x}) \end{pmatrix} \frac{1}{\omega - \varepsilon_\alpha + i\eta} \begin{pmatrix} \bar{U}_\alpha(\vec{y}) \\ \bar{V}_\alpha(\vec{y}) \end{pmatrix} \\ & + \sum_\beta \begin{pmatrix} U_\beta(\vec{x}) \\ V_\beta(\vec{x}) \end{pmatrix} \frac{1}{\omega + \varepsilon_\beta - i\eta} \begin{pmatrix} \bar{U}_\beta(\vec{y}) \\ \bar{V}_\beta(\vec{y}) \end{pmatrix}. \end{aligned} \quad (24)$$

The components $U_{\alpha,\beta}$ and $V_{\alpha,\beta}$ are Dirac spinors corresponding to the normal and time-reversed components, respectively, of the positive-frequency, ε_α , and negative-frequency, ε_β , solutions to the Dirac-Gorkov equation

$$\int d^3y \begin{pmatrix} \gamma_0((\varepsilon + \mu)\delta(\vec{x} - \vec{y}) - h(\vec{x}, \vec{y})) & \Delta(\vec{x}, \vec{y}) \\ \bar{\Delta}(\vec{x}, \vec{y}) & ((\varepsilon - \mu)\delta(\vec{x} - \vec{y}) + h_T(\vec{x}, \vec{y}))\gamma_0 \end{pmatrix} \begin{pmatrix} U(\vec{y}) \\ V(\vec{y}) \end{pmatrix} = 0, \quad (25)$$

where we have introduced the single-particle hamiltonian, $h(\vec{x}, \vec{y})$, given by

$$h(\vec{x}, \vec{y}) = (-i\vec{\alpha} \cdot \vec{\nabla} + \beta M)\delta(\vec{x} - \vec{y}) + \beta\Sigma(\vec{x}, \vec{y}), \quad (26)$$

with

$$h_T(\vec{x}, \vec{y}) = Ah^T(\vec{x}, \vec{y})A^\dagger \quad \text{and} \quad h(\vec{x}, \vec{y}) = h^\dagger(\vec{x}, \vec{y}). \quad (27)$$

After multiplying on the left by the matrix $\begin{pmatrix} \gamma_0 & 0 \\ 0 & 1 \end{pmatrix}$, the Dirac-Gorkov equation, Eq. (25), can be written in Hamiltonian form as a Hermitian eigenequation,

$$\int d^3y \begin{pmatrix} (\varepsilon + \mu)\delta(\vec{x} - \vec{y}) - h(\vec{x}, \vec{y}) & \bar{\Delta}^\dagger(\vec{x}, \vec{y}) \\ \bar{\Delta}(\vec{x}, \vec{y}) & (\varepsilon - \mu)\delta(\vec{x} - \vec{y}) + h_T(\vec{x}, \vec{y}) \end{pmatrix} \begin{pmatrix} U(\vec{y}) \\ \gamma_0 V(\vec{y}) \end{pmatrix} = 0. \quad (28)$$

We thus conclude that the eigenvalues ε are real.

After multiplying the complex conjugate of Eq. (25) on the left by the matrix $\gamma_0 A \otimes \tau_1$, we can manipulate it into a form which is identical to the original equation, except for the sign of ε . We may thus conclude that the solutions to the Dirac-Gorkov equation occur in pairs with real eigenvalues of opposite sign and eigenvectors of the form,

$$\varepsilon = \varepsilon_\alpha : \begin{pmatrix} U(\vec{y}) \\ V(\vec{y}) \end{pmatrix}, \quad \varepsilon = -\varepsilon_\alpha : \begin{pmatrix} \gamma_0 AV^*(\vec{y}) \\ \gamma_0 AU^*(\vec{y}) \end{pmatrix}. \quad (29)$$

Using the above properties of the eigensolutions, we could rewrite the full HFB propagator of Eq. (24) as a sum over the positive eigenvalues ε_α alone. However, we will continue to use the form given in Eq. (24), distinguishing the positive and negative frequency solutions through explicit reference to one or the other.

In the frequency representation, the self-consistency equations take the form

$$\begin{aligned} \Sigma(\vec{x}, \vec{y}; \omega) = & -i\delta(\vec{x} - \vec{y}) \sum_j \Gamma_{j\alpha}(\vec{x}) \int d^3z D_j^{\alpha\beta}(\vec{x} - \vec{z}; 0) \int \frac{d\omega}{2\pi} \text{Tr} \left[\Gamma_{j\beta}(\vec{z}) G(\vec{z}, \vec{z}; \omega^+) \right] \\ & + i \sum_j \int \frac{d\omega'}{2\pi} \Gamma_{j\alpha}(\vec{x}) D_j^{\alpha\beta}(\vec{x} - \vec{y}; \omega - \omega') G(\vec{x}, \vec{y}; \omega') \Gamma_{j\beta}(\vec{y}), \end{aligned} \quad (30)$$

and

$$\Delta(\vec{x}, \vec{y}; \omega) = i \sum_j \int \frac{d\omega'}{2\pi} \Gamma_{j\alpha}(\vec{x}) D_j^{\alpha\beta}(\vec{x} - \vec{y}; \omega - \omega') F(\vec{x}, \vec{y}; \omega') A \Gamma_{j\beta}^T(\vec{y}) A^\dagger, \quad (31)$$

where we have taken the vertices to be time independent and have assumed a time dependence of the form $t - t'$ in all other quantities. We evaluate the equations in the static limit of the meson propagators,

$$D^{\alpha\beta}(\vec{x} - \vec{y}; \omega) \longrightarrow D^{\alpha\beta}(\vec{x} - \vec{y}; 0) \equiv D^{\alpha\beta}(\vec{x} - \vec{y}). \quad (32)$$

We then have for the self-consistency equations

$$\begin{aligned} \Sigma(\vec{x}, \vec{y}) = & -i\delta(\vec{x} - \vec{y}) \sum_j \Gamma_{j\alpha}(\vec{x}) \int d^3z D_j^{\alpha\beta}(\vec{x} - \vec{z}) \int \frac{d\omega}{2\pi} \text{Tr} \left[\Gamma_{j\beta}(\vec{z}) G(\vec{z}, \vec{z}; \omega^+) \right] \\ & + i \sum_j \Gamma_{j\alpha}(\vec{x}) D^{\alpha\beta}(\vec{x} - \vec{y}) \int \frac{d\omega}{2\pi} G(\vec{x}, \vec{y}; \omega) \Gamma_{j\beta}(\vec{y}), \end{aligned} \quad (33)$$

and

$$\Delta(\vec{x}, \vec{y}) = i \sum_j \Gamma_{j\alpha}(\vec{x}) D_j^{\alpha\beta}(\vec{x} - \vec{y}) \int \frac{d\omega}{2\pi} F(\vec{x}, \vec{y}; \omega) A \Gamma_{j\beta}^T(\vec{y}) A^\dagger.$$

Finally, we evaluate the frequency integrals by closing the contour in the upper half-plane, yielding

$$\begin{aligned} \Sigma(\vec{x}, \vec{y}) = & \delta(\vec{x} - \vec{y}) \sum_j \Gamma_{j\alpha}(\vec{x}) \int d^3z D_j^{\alpha\beta}(\vec{x} - \vec{z}) \sum_{\varepsilon_\gamma < 0} \bar{U}_\gamma(\vec{z}) \Gamma_{j\beta}(\vec{z}) U_\gamma(\vec{z}) \\ & - \sum_j \Gamma_{j\alpha}(\vec{x}) D^{\alpha\beta}(\vec{x} - \vec{y}) \sum_{\varepsilon_\gamma < 0} U_\gamma(\vec{x}) \bar{U}_\gamma(\vec{y}) \Gamma_{j\beta}(\vec{y}), \end{aligned} \quad (34)$$

and

$$\Delta(\vec{x}, \vec{y}) = - \sum_j \Gamma_{j\alpha}(\vec{x}) D_j^{\alpha\beta}(\vec{x} - \vec{y}) \sum_{\varepsilon_\gamma < 0} U_\gamma(\vec{x}) \bar{V}_\gamma(\vec{y}) A \Gamma_{j\beta}^T(\vec{y}) A^\dagger, \quad (35)$$

where the sum runs over the negative frequency solutions, $\varepsilon_\gamma < 0$, of Eq. (25).

The expressions for the number of protons and neutrons can be written similarly as

$$\left. \begin{array}{l} Z \\ N \end{array} \right\} = \int d^3x \sum_{\varepsilon_\gamma < 0} U_\gamma^\dagger(\vec{x}) \frac{(1 \pm \tau_3)}{2} U_\gamma(\vec{x}). \quad (36)$$

The expression for the energy can be reduced to

$$\begin{aligned} E = & \int d^3x \left(\sum_{\varepsilon_\gamma < 0} U_\gamma^\dagger(\vec{x}) (\varepsilon_\gamma + \mu) U_\gamma(\vec{x}) - \frac{1}{6} g_3 \sigma(\vec{x})^3 - \frac{1}{4} g_4 \sigma(\vec{x})^4 \right) \\ & - \frac{1}{2} \int d^3x d^3y \sum_{\varepsilon_\gamma < 0} \left(\bar{U}_\gamma^\dagger(\vec{x}) \Sigma(\vec{x}, \vec{y}) U_\gamma(\vec{y}) - \bar{U}_\gamma^\dagger(\vec{x}) \Delta(\vec{x}, \vec{y}) V_\gamma(\vec{y}) \right), \end{aligned} \quad (37)$$

Note that the last term is real due to the hermiticity of the Dirac-Gorkov equation.

The summation over negative frequency solutions in Eqs. (34) through (37) takes into account the occupation of all states, both those in the Fermi sea (the surface of which is now diffuse, due to the pairing) and those in the Dirac sea. These expressions would thus require renormalization to yield finite results. Instead, we simply truncate the sums by excluding the solutions corresponding to quasi-particle states in the Dirac sea. This approximation has been found to give reasonable results in nuclear matter [29].

Before reducing the self-consistency equations, together with the Dirac-Gorkov equation, Eq. (25), to a form in which they can be solved, we observe that, with $B = \gamma_5 C$, each of the pair of wave vectors, $\begin{pmatrix} U(\vec{x}) \\ V(\vec{x}) \end{pmatrix}$ and $\begin{pmatrix} BU^*(\vec{x}) \\ BV^*(\vec{x}) \end{pmatrix}$, possesses the time-reversed Dirac structure of the other. In Appendix A, we show that when these two states are equally occupied, then they satisfy the same Dirac-Gorkov equation with the same eigenvalue. We will assume this to be the case in the following.

IV. REDUCING THE SELF-CONSISTENCY EQUATIONS

We begin by analyzing the isospin structure of the self-energy and pairing fields under the assumption of pure proton-proton and neutron-neutron pairing. In this case, the solutions to the Dirac-Gorkov equation will be either purely proton particle-hole ones or neutron particle-hole ones of the form

$$\Psi_p = \begin{pmatrix} U_p \\ 0 \\ 0 \\ V_p \end{pmatrix} \quad \text{and} \quad \Psi_n = \begin{pmatrix} 0 \\ U_n \\ V_n \\ 0 \end{pmatrix},$$

where each of the elements in the column vectors are themselves 4-component Dirac spinors. Substitution of these into the self-consistency equations yields isospin structures of the mean fields of the form

$$\Sigma(\vec{x}, \vec{y}) = \begin{pmatrix} \Sigma_p(\vec{x}, \vec{y}) & 0 \\ 0 & \Sigma_n(\vec{x}, \vec{y}) \end{pmatrix} \quad \text{and} \quad \Delta(\vec{x}, \vec{y}) = \begin{pmatrix} 0 & \Delta_p(\vec{x}, \vec{y}) \\ \Delta_n(\vec{x}, \vec{y}) & 0 \end{pmatrix}, \quad (38)$$

where each of the elements of the matrices are themselves 4x4 matrices. The isospin dependent Dirac-Gorkov equation thus decouples into independent equations for neutrons and protons. In their Hamiltonian form, these are

$$\int d^3y \begin{pmatrix} (\varepsilon + \mu_t)\delta(\vec{x} - \vec{y}) - h_t(\vec{x}, \vec{y}) & \bar{\Delta}_t^\dagger(\vec{x}, \vec{y}) \\ \bar{\Delta}_t(\vec{x}, \vec{y}) & (\varepsilon - \mu_t)\delta(\vec{x} - \vec{y}) + h_t(\vec{x}, \vec{y}) \end{pmatrix} \begin{pmatrix} U_t(\vec{y}) \\ \gamma_0 V_t(\vec{y}) \end{pmatrix} = 0, \quad (39)$$

where we have written the respective Dirac hamiltonian operators as

$$h_t(\vec{x}, \vec{y}) = (-i\vec{\alpha} \cdot \vec{\nabla} + \beta M)\delta(\vec{x} - \vec{y}) + \beta \Sigma_t(\vec{x}, \vec{y}) \quad t = p, n \quad (40)$$

and the Lagrange multipliers as $\mu_p = \mu + \delta\mu$ and $\mu_n = \mu - \delta\mu$. We have also made use of the fact that $\Sigma_{tT}(\vec{x}, \vec{y}) = \Sigma_t(\vec{x}, \vec{y})$, so that $h_{tT}(\vec{x}, \vec{y}) = h_t(\vec{x}, \vec{y})$, since we have assumed invariance under time inversion of the Dirac structure.

We want to obtain the coupled equations for the case of an axially-deformed nucleus. We take the z-axis to be the symmetry axis and use cylindrical coordinates ($x = r_\perp \cos \varphi$, $y = r_\perp \sin \varphi$, and z). Although the total angular momentum j is no longer a good quantum number, its projection along the symmetry axis Ω , as well as the parity π , (and, of course, the isospin projection, which we also denote by t) are still good quantum numbers. We write each of the 4-component spinors of the wave-function as

$$U_{t\gamma}(\vec{x}) = \begin{pmatrix} u f_{t\gamma}(\vec{x}) \\ i u g_{t\gamma}(\vec{x}) \end{pmatrix} = \frac{1}{\sqrt{2\pi}} \begin{pmatrix} u f_{t\gamma}^+(r_{\perp}, z) e^{i(\Omega_{\gamma}-1/2)\varphi} \\ u f_{t\gamma}^-(r_{\perp}, z) e^{i(\Omega_{\gamma}+1/2)\varphi} \\ i u g_{t\gamma}^+(r_{\perp}, z) e^{i(\Omega_{\gamma}-1/2)\varphi} \\ i u g_{t\gamma}^-(r_{\perp}, z) e^{i(\Omega_{\gamma}+1/2)\varphi} \end{pmatrix}, \quad (41)$$

and

$$\gamma_0 V_{t\gamma}(\vec{x}) = \begin{pmatrix} v f_{t\gamma}(\vec{x}) \\ i v g_{t\gamma}(\vec{x}) \end{pmatrix} = \frac{1}{\sqrt{2\pi}} \begin{pmatrix} v f_{t\gamma}^+(r_{\perp}, z) e^{i(\Omega_{\gamma}-1/2)\varphi} \\ v f_{t\gamma}^-(r_{\perp}, z) e^{i(\Omega_{\gamma}+1/2)\varphi} \\ i v g_{t\gamma}^+(r_{\perp}, z) e^{i(\Omega_{\gamma}-1/2)\varphi} \\ i v g_{t\gamma}^-(r_{\perp}, z) e^{i(\Omega_{\gamma}+1/2)\varphi} \end{pmatrix}, \quad (42)$$

in which the functions $u f_{t\gamma}^{\pm}$, $u g_{t\gamma}^{\pm}$, $v f_{t\gamma}^{\pm}$, and $v g_{t\gamma}^{\pm}$ are real. For each solution with positive value of the angular momentum projection, Ω_{γ} , we have a time-reversed solution with the same energy but a negative value of the angular momentum projection, $-\Omega_{\gamma}$, given by $B U_{t\gamma}^*(\vec{x})$ and $\gamma_0 B V_{t\gamma}^*(\vec{x})$. The densities that enter the Hartree terms of the self-energy can then be written as

$$\begin{aligned} \rho_s(r_{\perp}, z) &= 2 \sum_{\omega_{t\gamma} < 0, t, \Omega_{\gamma} > 0} U_{t\gamma}^{\dagger} \gamma_0 U_{t\gamma}, \\ \rho_B(r_{\perp}, z) &= 2 \sum_{\omega_{t\gamma} < 0, t, \Omega_{\gamma} > 0} U_{t\gamma}^{\dagger} U_{t\gamma}, \\ \rho_3(r_{\perp}, z) &= 2 \sum_{\omega_{t\gamma} < 0, t, \Omega_{\gamma} > 0} 2m_t U_{t\gamma}^{\dagger} U_{t\gamma}, \\ \rho_c(r_{\perp}, z) &= 2 \sum_{\omega_{t\gamma} < 0, t, \Omega_{\gamma} > 0} (m_t + 1/2) U_{t\gamma}^{\dagger} U_{t\gamma}, \end{aligned} \quad (43)$$

in which the sum over states of different parity is implicit in the sum over states of different energy. The local Hartree contribution to the self-energy may be written in terms of these densities as

$$\begin{aligned} \beta \Sigma_H(\vec{x}, \vec{y}) &= \delta(\vec{x} - \vec{y}) \int d^3 z \left(-\beta g_{\sigma}^2 d_{\sigma}(\vec{x} - \vec{z}) \rho_s(\vec{z}) + g_{\omega}^2 d_{\omega}^0(\vec{x} - \vec{z}) \rho_B(\vec{z}) \right. \\ &\quad \left. + \left(\frac{g_{\rho}}{2} \right)^2 \tau_3 d_{\rho}^0(\vec{x} - \vec{z}) \rho_3(\vec{z}) + e^2 \frac{(1 + \tau_3)}{2} d_{\gamma}^0(\vec{x} - \vec{z}) \rho_c(\vec{z}) \right), \end{aligned} \quad (44)$$

where the meson propagators have been reduced to

$$d_j^0(\vec{x} - \vec{z}) = \frac{1}{4\pi} \frac{\exp(-m_j |\vec{x} - \vec{z}|)}{|\vec{x} - \vec{z}|}, \quad (45)$$

with the exception of the σ -meson propagator, which is still assumed to contain the nonlinear terms. It is customary to write the Hartree contribution to the self-energy in terms of the mean fields associated with each of the mesons, as

$$\beta \Sigma_H(\vec{x}) = -\beta g_{\sigma} \sigma(\vec{x}) + g_{\omega} \omega^0(\vec{x}) + \frac{g_{\rho}}{2} \tau_3 \rho^{00}(\vec{x}) + e \frac{(1 + \tau_3)}{2} A^0(\vec{x}), \quad (46)$$

with

$$\begin{aligned}
\omega^0(\vec{x}) &= g_\omega \int d^3z d_\omega^0(\vec{x} - \vec{z}) \rho_B(\vec{z}), \\
\rho^{00}(\vec{x}) &= \frac{g_\rho}{2} \int d^3z d_\rho^0(\vec{x} - \vec{z}) \rho_3(\vec{z}), \\
A^0(\vec{x}) &= e \int d^3z d_\gamma^0(\vec{x} - \vec{z}) \rho_c(\vec{z}), \\
\sigma(\vec{x}) &= g_\sigma \int d^3z d_\sigma(\vec{x} - \vec{z}) \rho_s(\vec{z}) \\
&= \int d^3z d_\sigma^0(\vec{x} - \vec{z}) \left(g_\sigma \rho_s(\vec{z}) - g_3 \sigma(\vec{x})^2 - g_4 \sigma(\vec{x})^3 \right).
\end{aligned} \tag{47}$$

In the last expression, we have written the σ mean field in terms of its free propagator, as given in Eq. (45), and included the nonlinear terms explicitly. The mean meson fields possess the same axial symmetry as the densities.

The Fock exchange term of the self-energy has the form

$$\begin{aligned}
\Sigma_F(\vec{x}, \vec{y}) &= - \sum_j \Gamma_{j\alpha}(\vec{x}) D^{\alpha\beta}(\vec{x} - \vec{y}) \\
&\times \sum_{\varepsilon_{t\gamma} < 0, t, \Omega_\gamma > 0} \chi_t \chi_t^\dagger \left(U_{t\gamma}(\vec{x}) U_{t\gamma}^\dagger(\vec{y}) + B U_{t\gamma}^*(\vec{x}) U_{t\gamma}^T(\vec{y}) B^\dagger \right) \gamma_0 \Gamma_{j\beta}(\vec{y}),
\end{aligned} \tag{48}$$

where we have written the isospin dependence of the intermediate states in terms of the isospinor χ_t . As has been discussed in the literature (cf. Ref. [7] or Ref. [42]), the most important effects of the Fock terms due to the exchange of the short-range σ , ω , and ρ mesons can be taken into account by using adjusted Hartree terms. This can be better understood by looking at the zero-range limit of the meson propagators, for which the Fock terms reduce to linear combinations of the Hartree ones. Here, we retain the small but finite range of the meson propagators, but approximate the self-energy as the Hartree contribution alone and use the parameters appropriate for this purpose.

The pairing field arises from an exchange term, similar in form to the Fock term of the self-energy. We can write it as

$$\begin{aligned}
\Delta(\vec{x}, \vec{y}) &= - \sum_j \Gamma_{j\alpha}(\vec{x}) D_j^{\alpha\beta}(\vec{x} - \vec{y}) \\
&\times \sum_{\varepsilon_{t\gamma} < 0, t, \Omega_\gamma > 0} \chi_t \chi_{\bar{t}} \left(U_{t\gamma}(\vec{x}) V_{t\gamma}^\dagger(\vec{y}) + B U_{t\gamma}^*(\vec{x}) V_{t\gamma}^T(\vec{y}) B^\dagger \right) \gamma_0 A \Gamma_{j\beta}^T(\vec{y}) A^\dagger,
\end{aligned} \tag{49}$$

where $\chi_{\bar{p}, \bar{n}} = \chi_{n, p}$ are the time-reversed isospinors.

We neglect the Coulomb contribution to the pairing field here and approximate the contributions of the other mesons using the zero-range (infinite-mass) limit of the meson propagators. We also neglect the contribution of the non-linear σ -meson terms. As we have argued in the introduction, due to the short range of the exchanged mesons, a zero-range approximation to their propagators does not make a significant difference in the results. It also greatly simplifies the numerical calculations. The Hamiltonian form of the pairing field is, in this case,

$$\begin{aligned}
\bar{\Delta}_t^\dagger(\vec{x}, \vec{y}) &= \gamma_0 \Delta_t(\vec{x}, \vec{y}) \gamma_0 \\
&= \delta(\vec{x} - \vec{y}) c_{pair} \left(\frac{g_\sigma^2}{m_\sigma^2} \gamma_0 \kappa_t(\vec{x}) \gamma_0 - \left(\frac{g_\omega^2}{m_\omega^2} + \frac{(g_\rho/2)^2}{m_\rho^2} \right) \gamma_0 \gamma^\mu \kappa_t(\vec{x}) \gamma_\mu \gamma_0 \right),
\end{aligned} \tag{50}$$

where the anomalous density $\kappa_t(\vec{x})$ is

$$\kappa_t(\vec{x}) = \sum_{\varepsilon_{t\gamma} < 0, \Omega_\gamma > 0} \left(U_{t\gamma}(\vec{x}) V_{t\gamma}^\dagger(\vec{x}) + B U_{t\gamma}^*(\vec{x}) V_{t\gamma}^T(\vec{x}) B^\dagger \right) \gamma_0 \quad t = p, n. \quad (51)$$

However, the pairing field, in the given form, does not necessarily satisfy the antisymmetry condition of Eq. (6). Applying the antisymmetry condition to the pairing field, we can reduce it to a condition on the anomalous density,

$$\kappa_t(\vec{x}) = B \kappa_t^T(\vec{x}) B^\dagger. \quad (52)$$

To ensure that this is satisfied, we take the anomalous density to be

$$\begin{aligned} \kappa_t(\vec{x}) &\rightarrow \frac{1}{2} \left(\kappa_t(\vec{x}) + B \kappa_t^T(\vec{x}) B^\dagger \right) \quad t = p, n \\ &= \frac{1}{2} \sum_{\varepsilon_{t\gamma} < 0, \Omega_\gamma > 0} \left(U_{t\gamma}(\vec{x}) V_{t\gamma}^\dagger(\vec{x}) \gamma_0 + B U_{t\gamma}^*(\vec{x}) V_{t\gamma}^T(\vec{x}) B^\dagger \gamma_0 \right. \\ &\quad \left. + \gamma_0 V_{t\gamma}(\vec{x}) U_{t\gamma}^\dagger(\vec{x}) + \gamma_0 B V_{t\gamma}^*(\vec{x}) U_{t\gamma}^T(\vec{x}) B^\dagger \right). \end{aligned} \quad (53)$$

We then write the components of the pairing field as

$$\bar{\Delta}_t^\dagger(\vec{x}) = \begin{pmatrix} \delta_{1t}(r_\perp, z) & 0 & i \delta_{3t}(r_\perp, z) & i \delta_{4t}(r_\perp, z) e^{-i\varphi} \\ 0 & \delta_{1t}(r_\perp, z) & i \delta_{4t}(r_\perp, z) e^{i\varphi} & -i \delta_{3t}(r_\perp, z) \\ -i \delta_{3t}(r_\perp, z) & -i \delta_{4t}(r_\perp, z) e^{-i\varphi} & \delta_{2t}(r_\perp, z) & 0 \\ -i \delta_{4t}(r_\perp, z) e^{i\varphi} & i \delta_{3t}(r_\perp, z) & 0 & \delta_{2t}(r_\perp, z) \end{pmatrix}, \quad (54)$$

where the four real functions δ_{jt} are

$$\begin{aligned} \delta_{1t}(r_\perp, z) &= (c_s - c_v) \kappa_{1t}(r_\perp, z) - 3c_v \kappa_{2t}(r_\perp, z), \\ \delta_{2t}(r_\perp, z) &= (c_s - c_v) \kappa_{2t}(r_\perp, z) - 3c_v \kappa_{1t}(r_\perp, z), \\ \delta_{3t}(r_\perp, z) &= (c_s + 2c_v) \kappa_{3t}(r_\perp, z), \\ \delta_{4t}(r_\perp, z) &= (c_s + 2c_v) \kappa_{4t}(r_\perp, z), \end{aligned} \quad (55)$$

with

$$c_s = c_{pair} \frac{g_\sigma^2}{m_\sigma^2} \quad \text{and} \quad c_v = c_{pair} \left(\frac{g_\omega^2}{m_\omega^2} + \frac{(g_\rho/2)^2}{m_\rho^2} \right). \quad (56)$$

The four real components of the anomalous density are

$$\begin{aligned} \kappa_{1t}(r_\perp, z) &= \sum_{\varepsilon_{t\gamma} < 0, \Omega_\gamma > 0} \left(u f_{t\gamma}^+ v f_{t\gamma}^+ + u f_{t\gamma}^- v f_{t\gamma}^- \right), \\ \kappa_{2t}(r_\perp, z) &= \sum_{\varepsilon_{t\gamma} < 0, \Omega_\gamma > 0} \left(u g_{t\gamma}^+ v g_{t\gamma}^+ + u g_{t\gamma}^- v g_{t\gamma}^- \right), \\ \kappa_{3t}(r_\perp, z) &= \frac{1}{2} \sum_{\varepsilon_{t\gamma} < 0, \Omega_\gamma > 0} \left(u f_{t\gamma}^+ v g_{t\gamma}^+ - u f_{t\gamma}^- v g_{t\gamma}^- + u g_{t\gamma}^+ v f_{t\gamma}^+ - u g_{t\gamma}^- v f_{t\gamma}^- \right), \\ \kappa_{4t}(r_\perp, z) &= \frac{1}{2} \sum_{\varepsilon_{t\gamma} < 0, \Omega_\gamma > 0} \left(u f_{t\gamma}^+ v g_{t\gamma}^- + u f_{t\gamma}^- v g_{t\gamma}^+ + u g_{t\gamma}^+ v f_{t\gamma}^- + u g_{t\gamma}^- v f_{t\gamma}^+ \right). \end{aligned} \quad (57)$$

The Dirac structure of the pairing field is very similar to that of the 1S_0 pairing field in symmetric nuclear matter, where

$$\Delta_{nm}(k) = \gamma_0 \Delta_{nm}^{-\dagger}(k) \gamma_0 = \Delta_S(k) - \gamma_0 \Delta_0(k) - i\gamma_0 \vec{\gamma} \cdot \vec{k} \Delta_T(k). \quad (58)$$

The upper and lower diagonal components of the pairing field, δ_{1t} and δ_{2t} can be directly associated with the linear combinations $\Delta_S \pm \Delta_0$ of the nuclear matter components, while the remaining components, δ_{3t} and δ_{4t} are more loosely related to the contributions of the nuclear matter tensor term, Δ_T .

An overall constant c_{pair} has been introduced in the expression for the pairing field to compensate for deficiencies of the interaction parameters and of the numerical calculation. The necessity for such a constant is apparent from studies of pairing in nuclear matter. Non-relativistic [46–48] and relativistic [31] calculations have verified that 1S_0 pairing in nuclear matter is dominated by the two-nucleon 1S_0 virtual state. Pairing in nuclear matter is weaker the further the 1S_0 virtual state is from the real axis in the complex-momentum plane. The location of the virtual state depends on the strength and form of the two-nucleon interaction and on the space of states used in the calculation. In Ref. [31], various sets of interaction parameters, even zero-range ones, were shown to furnish mutually consistent physical values for the pairing gap function, when they were supplemented with a large momentum cutoff adjusted so as to place the two-nucleon virtual state at its physical location. We expect a condition similar to that in nuclear matter to apply here. However, as it is extremely difficult to fix the position of the two-nucleon virtual state within the harmonic oscillator basis that we use, we instead multiply the pairing field by an overall constant that we expect to be able to fix independently of the charge and mass of the systems under consideration. We emphasize that this is not a weakness of our calculations alone, but of any Hartree-(Fock)-Bogoliubov calculation using a limited space of states and an effective interaction, even those using a finite-range one. The pairing field obtained in such a calculation will depend on both the interaction and the space of states used and will usually require that one or the other of these be adjusted in order to obtain reasonable results. Here, we find it more convenient to introduce an arbitrary constant in the interaction rather than arbitrarily limit the space of states we use.

With the above simplifications in the self-energy and pairing fields, the Dirac-Gorkov equations for neutrons and protons reduce to local differential equations. Their Hamiltonian form is

$$\begin{pmatrix} \varepsilon + \mu_t - h_t(\vec{x}) & \bar{\Delta}_t^\dagger(\vec{x}) \\ \bar{\Delta}_t(\vec{x}) & \varepsilon - \mu_t + h_t(\vec{x}) \end{pmatrix} \begin{pmatrix} U_t(\vec{x}) \\ \gamma_0 V_t(\vec{x}) \end{pmatrix} = 0, \quad (59)$$

with

$$h_t(\vec{x}) = -i\vec{\alpha} \cdot \vec{\nabla} + \beta M^*(\vec{x}) + V_t(\vec{x}) \quad t = p, n, \quad (60)$$

where

$$\begin{aligned} M^*(\vec{x}) &= M - g_\sigma \sigma(\vec{x}), \\ V_t(\vec{x}) &= g_\omega \omega^0(\vec{x}) + \frac{g_\rho}{2} 2m_t \rho^{00}(\vec{x}) + e(1/2 + m_t) A^0(\vec{x}), \end{aligned} \quad (61)$$

and $\bar{\Delta}_t^\dagger(\vec{x})$ is given in Eq. (54).

The total energy can now be written in terms of the mean fields as

$$E = \int d^3x \left(\sum_{\varepsilon_\gamma < 0} |U_\gamma(\vec{x})|^2 (\varepsilon_\gamma + \mu) - \frac{1}{6} g_3 \sigma(\vec{x})^3 - \frac{1}{4} g_4 \sigma(\vec{x})^4 + \frac{1}{2} g_\sigma \sigma(\vec{x}) \rho_s(\vec{x}) \right. \\ \left. - \frac{1}{2} g_\omega \omega^0(\vec{x}) \rho_B(\vec{x}) - \frac{1}{2} \frac{g_\rho}{2} \rho^{00}(\vec{x}) \rho_3(\vec{x}) - \frac{1}{2} e A^0(\vec{x}) \rho_c(\vec{x}) + \frac{1}{2} \sum_t \text{Tr}[\bar{\Delta}_t^\dagger(\vec{x}) \kappa_t(\vec{x})] \right) \\ - E_{cm}. \quad (62)$$

In the expression above, we have also subtracted the harmonic oscillator estimate to the center-of-mass motion,

$$E_{cm} = \frac{3}{4} \hbar \omega_0 = \frac{3}{4} \frac{41}{A^{1/3}} \text{ MeV}, \quad (63)$$

in order to obtain an expression for the total internal energy of the nucleus.

V. NUMERICAL SOLUTION OF THE DHB EQUATION

We solve the Dirac-Gorkov and the Klein-Gordon equations by expanding the fields as well as the wavefunctions in complete sets of eigenfunctions of harmonic oscillator potentials. In actual calculations, the expansion is truncated at a finite number of major shells, with the quantum number of the last included shell denoted by N_F in the case of the fermions and by N_B for the bosons. The maximum values are selected so as to assure the physical significance of the results obtained. The same procedure has been used by many researchers, among them, by Vautherin [49] in the nonrelativistic Hartree-Fock approximation, by Ghambir et al. [17] in the relativistic mean field + BCS approach and by Lalazissis et al. [40–42] in the RHB approach.

The spinors of the Dirac-Gorkov equation are expanded in terms of the eigenfunctions of an axially-deformed harmonic-oscillator potential,

$$V_{osc}(r_\perp, z) = \frac{1}{2} M \omega_z^2 z^2 + \frac{1}{2} M \omega_\perp^2 r^2. \quad (64)$$

The oscillator constants are taken as

$$\beta_z = \frac{1}{b_z} = \sqrt{\frac{M \omega_z}{\hbar}} \quad \beta_\perp = \frac{1}{b_\perp} = \sqrt{\frac{M \omega_\perp}{\hbar}}. \quad (65)$$

with volume conservation relating the two constants to that of a spherically-symmetric potential $b_\perp^2 b_z = b_0^3$.

The eigenfunctions of the deformed harmonic oscillator can be written explicitly as,

$$\Phi_\alpha(\vec{r}) = \psi_{n_r}^{m_l}(r_\perp) \psi_{n_z}(z) \frac{e^{i m_l \varphi}}{\sqrt{2\pi}} \chi_{m_s} \chi_{m_t} \quad (66)$$

where α denotes the complete set of quantum numbers (n_r , m_l , n_z , m_s , and m_t) and

$$\begin{aligned}\psi_{n_r}^{m_l}(r_\perp) &= \frac{N_{n_r}^{m_l}}{b_\perp} \sqrt{2} \eta^{m_l/2} L_{n_r}^{m_l}(\eta) e^{-\eta/2} & \text{with} & \quad \eta = \left(\frac{r}{b_\perp}\right)^2 \\ \psi_{n_z}(z) &= \frac{N_{n_z}}{\sqrt{b_z}} H_{n_z}(\xi) e^{-\xi^2/2} & \text{with} & \quad \xi = \frac{z}{b_z}\end{aligned}\quad (67)$$

In Eq. (67), $L_{n_r}^{m_l}(\eta)$ and $H_{n_z}(\xi)$ are Hermite and associate Laguerre polynomials [50], with the normalization constants, $N_{n_r}^{m_l}$ and N_{n_z} , given in Ref. [17]. In these equations, n_r and n_z are the number of nodes in the r and z directions, and m_l and m_s are the projections of angular momentum and spin on the z axis. The third component of the total angular momentum Ω_γ and the parity π are then defined as,

$$\Omega_\gamma = m_l + m_s \quad \pi = (-1)^{n_z+m_l}. \quad (68)$$

We expand the Pauli components of the Dirac spinors, $uf_{t\gamma}(r_\perp, z)$, $ug_{t\gamma}(r_\perp, z)$, $vf_{t\gamma}(r_\perp, z)$, and $vg_{t\gamma}(r_\perp, z)$, in terms of the oscillator eigenfunctions. Inserting these expansions into the Dirac-Gorkov equation Eq. (59), we can reduce the equation to the diagonalization problem of a symmetric matrix and calculate the Hartree densities of Eq. (43) and components of the anomalous density of Eq. (57). The fields of the massive mesons are expanded in a manner similar to the fermion expansion, with the same deformation parameter β_0 but a smaller oscillator length of $b_B = b_0/\sqrt{2}$. The Coulomb field is calculated directly in configuration space. In short, the method used is a direct generalization of that described in Ref. [17], where more details may be found.

VI. NUMERICAL RESULTS

The parameters required to perform numerical calculations are the nucleon and meson masses, the meson-nucleon coupling constants and the factor c_{pair} that multiplies the pairing interaction. The calculations that we present were performed using the masses and coupling constants of the NL3 potential [51]. We performed calculations for several values of the factor c_{pair} . These permit us to study the extent to which physical observables depend on the pairing interaction and to choose the value of the parameter c_{pair} that best fits the observables.

As the mesons fields and the nucleon wavefunctions are expanded in a deformed basis of harmonic oscillator states, we must also specify the number of major oscillator shells to be used in the expansions for fermions, N_F , and bosons, N_B , as well as the basis deformation parameter, β_0 . Here, we work, for the most part, in a basis of 12 major oscillator shells for fermions and 24 for bosons. We use the standard expression for the oscillator frequencies, $\hbar\omega_0 = 41A^{-1/3}$ MeV, and spherical bases, with $\beta_0 = 0$, in all calculations. Although the number of major oscillator shells is not as large as might be desired, it does seem to be large enough to obtain reasonable values for the observables studied.

In order to analyze the characteristics of the single-particle levels, we define several related average values. First, in deference to the standard nonrelativistic notation, we define the occupation probability of each of the two states of the level with frequency $\varepsilon_{t\gamma} < 0$ as

$$v_{t\gamma}^2 = \int d^3x |U_{t\gamma}(\vec{x})|^2, \quad (69)$$

so that we also have

$$u_{t\gamma}^2 = 1 - v_{t\gamma}^2 = \int d^3x |V_{t\gamma}(\vec{x})|^2. \quad (70)$$

We define the energy of a single-particle level as

$$E_{t\gamma} = \int d^3x \left(U_{t\gamma}^\dagger(\vec{x}) h_t U_{t\gamma}(\vec{x}) + V_{t\gamma}^\dagger(\vec{x}) h_t V_{t\gamma}(\vec{x}) \right), \quad (71)$$

in which we take advantage of the normalization of the state vector to avoid normalizing the result. This is not possible for the pairing term, for which we define the gap parameter of a single-particle level as

$$\Delta_{t\gamma} = - \int d^3x U_{t\gamma}^\dagger(\vec{x}) \bar{\Delta}_t^\dagger \gamma_0 V_{t\gamma}(\vec{x}) / u_{t\gamma} v_{t\gamma}. \quad (72)$$

The definition of the gap parameter is fragile and is subject to numerical error when $v_{t\gamma} \rightarrow 1$ or $u_{t\gamma} \rightarrow 1$. We define an average gap parameter for the neutrons and protons of a nucleus as

$$\langle \Delta_t \rangle = \sum_{\varepsilon_\gamma < 0} \Delta_{t\gamma} v_{t\gamma}^2 / \sum_{\varepsilon_\gamma < 0} v_{t\gamma}^2. \quad (73)$$

We note that, unlike in the BCS approximation, no relation exists here between the occupation probabilities, $v_{t\gamma}^2$ and $u_{t\gamma}^2$, the energy $E_{t\gamma}$, and the gap parameter $\Delta_{t\gamma}$. However, these averages still furnish a good description of the most important characteristics of the single-particle levels.

In the following, we first analyze pairing in the isotopes of tin and then discuss similar results for the isotopes of nickel and calcium, all of which are spherical. The isotopes of tin and nickel have already been the object of two thorough studies [40,52]. We then analyze deformation and pairing of the $N=28$ isotonic chain, which has been the object of two recent studies [42,58,59]. Finally, we turn our attention to nuclei in the region of the $Z \approx 40$ subshell closure, the isotopes of Kr and Sr, in particular. These have been the object of many previous studies. [20–22,54,55]

A. Spherical Nuclei

Pairing in the Sn and Ni isotopes has been studied extensively, due to the simplification provided by their spherical symmetry. In Ref. [52], Dobaczewski et al. describe a very complete study of pairing in the Sn isotopes, based on a nonrelativistic Hartree-Fock-Bogoliubov approximation, in which they examine the differences in pairing due to the use of various effective interactions and due to coupling to the particle continuum, as well as the effects of these on experimental observables. In Ref. [40], Lalazissis et al. compare RHB calculations of both the odd and even isotopes in the Sn and Ni chains with the experimental data, obtaining quite good agreement. In another study [38], Meng compared RHB calculations using the finite-range Gogny D1S and a zero-range interaction and found good agreement between the two and with the experimental data.

We begin our study of spherical nuclei with the tin isotopes. We performed calculations of the ground states of the even isotopes from ^{100}Sn to ^{176}Sn , that is, from the closed neutron shell at $N=50$ to the closed shell at $N=126$. We present calculations for three values of the parameter c_{pair} . The objective of this study was to identify the observables sensitive to the parameter c_{pair} (and, thus, to the pairing) and to adjust the parameter accordingly.

We present in Fig. 1 the two-neutron separation energy of the even Sn isotopes in the mass range from $A=100$ to $A=176$, calculated for the values $c_{pair}=0.45, 0.47$ and 0.50 . We compare our calculations with the two-neutron separation energies obtained using the ground state masses tables of Möller-Nix [56] and of Audi-Wapstra [57]. The Möller-Nix values for ground state masses were calculated using an extended finite-range droplet model with parameters adjusted to the experimental ground state masses. The Audi-Wapstra values for the ground state masses are essentially the experimental ones, with some extension to proton- and neutron-rich nuclei based on systematics. We verify that all three calculations follow the trend of the Möller-Nix and Audi-Wapstra values. The two-neutron separation energy is seen to be almost independent of the strength of the pairing field, with the calculation using $c_{pair}=0.50$ providing only slightly better agreement with the data than the others. All the calculations underestimate S_{2n} in the region of $A=100$. This discrepancy might be attributable to a deficiency in the isospin dependence of the NL3 parameter set. It could also be due to effects that are not included in the calculation, such as neutron-proton correlations, which are suspected of being of importance in $N \approx Z$ nuclei. Our two-neutron separation energies are in good agreement with the RHB ones of Ref. [40]. However, such consistency is to be expected, given the relative insensitivity of the two-neutron separation energy to the pairing, since both calculations use the NL3 parameter set.

The calculated two-neutron separation energies remain almost constant from the shell closure at $A=132$ to about $A=160$, in contrast to the Möller-Nix values, which decrease slowly. The SIII and Sk δ Skyrme interaction calculations of Ref. [52] also furnish a relatively constant separation energy above the $A=132$ shell closure, which extends to even higher values of the mass, although most of their calculations are in agreement with the Möller-Nix systematics. The nucleus ^{176}Sn is unbound in the calculation with $c_{pair}=0.50$, as it is in all of the calculations of Ref. [52]. In our calculations, this is due to the fact that ^{174}Sn is more tightly bound for $c_{pair}=0.50$ than for the other values of the parameter. The binding energy of the magic nucleus ^{176}Sn is the same for all values of the parameter c_{pair} .

In Fig. 2 we show the average value of the neutron gap parameter of the even Sn isotopes as a function of the mass number A , for the same three values of c_{pair} . The gap parameter possesses a clear dependence on the value of c_{pair} . We also show in the figure the Möller-Nix and experimental Audi-Wapstra values for the standard estimate of the neutron gap parameter as the difference between the binding energies of an even-even nucleus and its odd mass neighbors,

$$\langle \Delta_n(Z, A) \rangle = B(Z, A) - \frac{1}{2}(B(Z, A-1) + B(Z, A+1))$$

where $B(Z, A)$ is the binding energy. The calculation with $c_{pair}=0.50$ shows reasonable agreement with the Möller-Nix values in the region of the $N=82, A=132$, shell closure, but tends to underestimate the Möller-Nix values well below the shell closure and overestimate these values well above the shell closure.

The neutron shell closures at $N=50,82$, and 126 are clearly visible in Fig. 2. At each of values of the neutron number, calculated neutron gap parameter goes to zero. We note that the experimental gap parameter has maximum, rather than a minimum, at each shell closure, reflecting the local maximum of the binding energy that occurs there. Several subshell closures are also visible in the calculations, at values of the mass at which the gap parameter reaches a non-zero minimum. These occur at $N=58$, $A=108$, between the $1g7/2$ and $2d5/2$ levels, at $N=64$, $A=114$, between the $2d5/2$ level and the remaining levels of the $4\hbar\omega$ shell, and at $N=112$, $A=162$, between the $5\hbar\omega$ shell and the $1i13/2$ level. Subshell closures are more visible when the pairing interaction is weaker and, thus, more sensitive to the energy differences between the levels.

Average values of the neutron gap parameter of the even Sn isotopes obtained in RHB and nonrelativistic calculations were presented in Refs. [40] and [52], respectively. The calculations using the Gogny interaction, both the RHB and the nonrelativistic ones, furnish a large value of the gap parameter – above 2 MeV – and show no subshell structure. Were we to increase the strength of the pairing interaction so as to obtain similar values for the pairing gap, our calculations would also show no shell substructure in the average pairing gap. The nonrelativistic calculations of Ref. [52], using Skyrme pairing interactions produced results in closer agreement with ours. These calculations also show structure due to subshell closures, although the structure is different from that seen here, possibly due to differences in the spin-orbit splitting of the levels, due to the different mean fields.

In Fig. 3, we show the pairing energy of the even Sn isotopes as a function of the mass number, obtained using the same three values of c_{pair} . The pairing energy is defined as

$$E_{pr} = -\frac{1}{2} \sum_t \int dx^3 \text{Tr}[\bar{\Delta}_t^\dagger(\vec{x}) \kappa_t(\vec{x})],$$

where κ_t and $\bar{\Delta}_t^\dagger$ are given in Eqs. (53) and (54), respectively. We observe that the pairing energy E_{pr} displays a dependence on the parameter c_{pair} and a shell structure similar to those seen in Fig. 2 for the average gap parameter. However, E_{pr} is observable only through its effects on the binding energy, which diminishes its utility as a means of determining the parameter c_{pair} .

In Fig. 4 we present the difference between the calculated value of the binding energy of the even Sn isotopes and the Möller-Nix value, as a function of the mass, using the same three values of c_{pair} used before. We also present the difference between the calculated value for $c_{pair}=0.50$ and the Audi-Wapstra values, where the latter exist. In the mass range of the valley of stability, the difference between the two binding energies can be minimized, to a certain point, through an appropriate choice of c_{pair} . For the tin isotopes, a value of c_{pair} close to 0.50 seems to yield the best average agreement. A value much larger than this would destroy the good agreement obtained for the gap parameter of Fig. 2. However, a larger value of c_{pair} would smooth out the two dips in the binding energy difference that roughly follow the mass dependence of both the average gap parameter and the pairing energy. This would yield pairing gaps in better agreement with the Gogny D1S ones of Ref. [40]. We then might expect to be able to reduce the remaining discrepancy by adjusting the mean field parameters.

In Fig. 4, the calculated value of the binding energy is larger than the experimental/systematic values in the $N \approx Z$ region and reaches a difference of about 4 MeV for

the magic nucleus ^{100}Sn , a result which is independent of the value of c_{pair} . The sharp increase of the binding-energy difference for $N \approx Z$ is consistent with the discrepancies between the calculated and the Möller-Nix values of the two-neutron separation energy, shown in Fig. 1. We can attribute the discrepancies to deficiencies in the isospin dependence of the NL3 parameters. If we were to include neutron-proton pairing in the calculations, the difference would only increase as the pairing would bind even more the already overbound $N \approx 50$ nuclei. The large differences in binding energy on the neutron-heavy side of the curve could be due as much to deficiencies in the Möller-Nix systematics as in the NL3 parameters.

In Fig. 5 we present the deviation from the systematic value, $r_{n0}N^{1/3}$, of the root mean square neutron radius of the even isotopes of Sn, as a function of the mass. The deviation displays a clear minimum at the principal shell closure at $N=82$. Although the deviation also tends to decrease near the shell closures at $N=50$ and $N=126$, the effect of these more extreme shell closures is much smaller than that of the $N=82$ one, within the stability valley. The deviation from the systematic value also possesses a sharp maximum at $N=112$, between the $5\hbar\omega$ shell and the $1i13/2$ level. We recall that the average gap parameter and the pairing energy display a minimum at the same subshell closure. Other subshell closures also appear in the deviation of the radius, but only as changes in its slope. The deviation from the systematic value of the root mean square mass radius of the even Sn isotopes shows the same structure, but to a lesser degree, and is not shown here. The deviation from the systematic of the root mean square proton radius, which is also not shown, increases monotonically with the mass number.

We find that the deviations of the root mean square radii are almost independent of the parameter c_{pair} and, thus, of the pairing interaction. Slightly larger variations have been seen in a comparison between RHB and Hartee+BCS calculations [42]. Still, with the exception of a few very special nuclei, such as ^{11}Li , the root mean square radii of a nucleus would seem to be determined almost exclusively by its mean field.

As the second example of a spherical isotopic chain, we studied the even isotopes of nickel, performing calculations from ^{48}Ni , at the $N=20$ shell closure, to ^{100}Ni , two neutrons beyond the subshell closure at $N=70$. We again performed calculations for three values of the parameter c_{pair} , their values in this case being $c_{pair}=0.49$, 0.50 , and 0.52 . Here we wanted to verify the generality of the observations made in the case of the Sn isotopes.

The calculations of the two-neutron separation energy for the Ni isotopes describe the tendency of the data fairly well, reproducing the discontinuities in separation energy that occur at the shell closures at $N=28$ and $N=50$. The calculated values of the (two-neutron) separation energy are almost independent of the parameter c_{pair} and underestimate the mass dependence of the separation energy at very low and very high values of the neutron excess, as in the case of Sn. Not surprisingly, our values are in good agreement with the RHB ones of Ref. [40], which also use the NL3 parameter set. They also agree well with the results of Ref. [38], obtained with the NLSH parameter set [53], using Gogny D1S and density-dependent zero-range pairing interactions.

In Fig. 6, we present the mean value of the neutron gap parameter of the even Ni isotopes as a function of the mass, for the same three values of c_{pair} . Again, we find a clear dependence of the gap parameter on the value of c_{pair} . The calculation with $c_{pair}=0.52$ shows the best agreement with the Möller-Nix and Audi-Wapstra values in the region above the shell

closure at $N=28$, $A=56$. All of the calculations are in disagreement with the experimental/systematic values in the region of the magic number $N=28$. This again suggests that short-range neutron-proton correlations may be important when $N \approx Z$.

In Fig. 6, we note that the neutron gap parameter is zero at the neutron shell closures at $N=20$, 28, and 50. The subshell closures are more marked here than in the case of tin. For Ni, these appear at $N=40$, $A=68$, between the $3\hbar\omega$ shell and the $1g9/2$ level and at $N=70$, $A=98$, between the $4\hbar\omega$ shell and the $1i11/2$ level. As occurred in the calculations of the isotopes of Sn, the value of the average gap parameter at the subshell closures increases with c_{pair} .

Values of the average neutron gap parameter of the Ni isotopes between $N=28$ and $N=50$, obtained using the Gogny interaction in a RHB calculation, were presented in Ref. [40]. As in the case of Sn, the RHB calculation furnishes values of the gap parameter greater than 2.5 MeV, which are quite large. The calculation presents a subshell structure similar to that with $c_{pair}=0.52$ in Fig. 6, but almost 50% larger in magnitude.

As in the case of the Sn isotopes, the pairing energy of the even Ni isotopes reflects the shell structure and the dependence on c_{pair} observed in the average gap parameter, but furnishes no new information. The root mean square radii reflect the same shell structure, although with less clarity, and are almost independent of the value of c_{pair} .

We also examined the Ca isotope chain, performing calculations of the even isotopes of Ca from $N=8$, $A=28$, to $N=50$, $A=70$, for two values of the parameter c_{pair} . Comparisons between the two calculations and the Audi-Wapstra and Möller-Nix systematics resulted in conclusions similar to those obtained for the tin and nickel isotopes. In particular, the two-neutron separation energies were well described in the two calculations, which show almost no dependence on the parameter c_{pair} . A value of $c_{pair}=0.55$ best agrees with the gap parameters obtained from the Audi-Wapstra systematics, which, in this case, lie about 20% below the Möller-Nix values.

In summary, we found our calculations of the root mean square radii and the two-neutron separation energies of spherical nuclei to be relatively independent of the strength of the pairing interaction. As the experimental data for these quantities are well fit by the NL3 parameter set used here, it is not surprising that our calculations describe them well. We observed that the pairing energy is only observable through its effects on the binding energy and that our calculations are not as successful at describing the latter as they are with the radii and the separation energies. A reasonable fit to the binding energies will depend on the adequate choice of the parameter c_{pair} as well as further adjustments in other interaction parameters. We found that the binding energy and the mean value of the gap parameter, to a certain point, are the observables that can be used as guides to a study of pairing in spherical nuclei.

B. Several deformed light nuclei

In this section, we analyze pairing and deformation in the $N = 28$ isotonic chain. The measured quadrupole deformations for these nuclei characterize ^{48}Ca as spherical but ^{46}Ar and ^{44}S as deformed, implying suppression of the $N = 28$ magic number. The deformation can be explained, in this case, by the close proximity of the $1f7/2$ level to the $2p$ levels in

the $4\hbar\omega$ shell. In the nucleus ^{48}Ca , the spherical proton configuration constrains the neutron configuration to also remain spherical. In the ^{46}Ar and ^{44}S nuclei, the partially filled proton shell perturbs the neutrons sufficiently for them to prefer a deformed configuration in which the $1f7/2$ and $2p$ orbitals are partially occupied.

Recent theoretical studies describe the experimental data for these nuclei reasonably well with nonrelativistic and relativistic mean field + BCS [58,59] calculations and with RHB calculations using the Gogny potential [42]. In Refs. [58] and [59], Werner et al. use both a Skyrme-Hartree-Fock approach and a relativistic mean field model, with the NLSH parameter set, to study various isotopic chains in the $N \approx 28$ region. They include pairing as a small (75 keV) constant pairing gap in a BCS formalism. They found the isotones ^{42}Si , ^{44}S and ^{46}Ar to show evidence of shape coexistence in both approaches, although the deformation at the energy minimum and its energy difference with the excited minimum varied between the two calculations. Lalazissis et al. used the RHB approach to perform a similar study of the $N \approx 28$ isotopes in Ref. [42]. Using the NL3 parameter set, they studied the even isotopes of Mg through Cr. They observed prolate-oblate staggering in the $N = 28$ isotones below ^{48}Ca , similar to that seen in the RMF calculations of Werner et al. and similar signs of shape coexistence: the binding energies versus quadrupole deformation of the isotones display two minima or a very flat single minimum.

We present here the average values of the gap parameter of the even-even S isotopes, in Fig. 7 as a function of the mass, for two values of the parameter c_{pair} . We observe that both calculations fall well below the Möller-Nix and Audi-Wapstra values at lower values of the mass. However, the isotopes that are of interest at the moment are in the region of large neutron excess, $A \gtrsim 40$, where the average values of the calculated gap parameter and the experimental/systematic values are in reasonable agreement. In particular, we see in Fig. 7, that the Möller-Nix and Audi-Wapstra values of the gap in ^{44}S fall close to the calculation with $c_{pair}=0.55$. The average value of the gap parameters of the other isotopes that we will examine show the same reasonable agreement with the experimental/systematic values in the mass range of interest.

To study in detail the dependence of the binding energy on the quadrupole deformation, we perform calculations at several fixed values of the deformation. To do this, we include in the Lagrangian a term that is quadratic in the difference between the quadrupole moment of the nucleus and the desired value of the moment. The solution of the equation of motion including this additional potential term tends to take a value which minimizes its contribution, thereby yielding a quadrupole moment close to the desired value. The contribution of the constraint term to the energy is subtracted to obtain the binding energy of the system at the value of the quadrupole moment obtained in the calculation. The consistency of the method can be verified by calculating the ground state energy of a spherical nucleus as a function of the quadrupole deformation β . For the case of ^{48}Ca , we find that the ground state energy reaches its minimum at $\beta = 0$, where the nucleus is spherical, just as we would expect. We also find a small difference of about 0.5 MeV between the calculations for the two values of c_{pair} . This difference is consistent with the small difference in the pairing energy and the small, but nonzero, average pairing gap found in the calculations.

In Fig. 8, we present the dependence on the deformation β of the binding energy of the nucleus ^{44}S , for the two values of c_{pair} . (The energy E_b displayed in the figure actually differs by a sign from the binding energy, $E_b(Z, A) = -B(Z, A)$.) Here the variation of c_{pair} from

0.50 to 0.55 makes a difference of almost 3 MeV in the binding energy, in contrast with the small difference of about 0.5 MeV found for ^{48}Ca . The energy curves for ^{44}S possess two well defined minima, with the oblate minimum about 1 MeV above the prolate one in the case of $c_{pair}=0.50$ and about 0.5 MeV above the prolate minimum when $c_{pair}=0.55$. The increase in the parameter c_{pair} tends to flatten the energy curve, thereby diminishing the differences between its peaks and valleys. The increase in c_{pair} also reduces the value of the deformation at the minima. The deformation at the oblate minimum decreases in magnitude by almost 20% with the increase of c_{pair} from 0.50 to 0.55, while the deformation at the prolate minimum is reduced by about 10% with the same increase in c_{pair} .

The experimental value of the quadrupole deformation of ^{44}S is $\beta=0.258(36)$ [60,61], which is in good agreement with the calculated value, $\beta=0.28$, using $c_{pair}=0.55$. The relativistic calculations of Werner et al. and Lalazissis et al. furnish a value of the deformation similar to this one. The RHB calculation of Ref. [42] yields an oblate minimum about 200 keV above the prolate one, which can be compared to our value of about 0.5 MeV between the two minima and a value of about 0.8 MeV in the RMF+BCS calculation of Refs. [58] and [59]. Nonrelativistic HF calculations furnish a value of β that is about half of the experimental one [58,59].

In Fig. 9, we present the dependence on the deformation β of the binding energy of the nucleus ^{46}Ar , for two values of the parameter c_{pair} . The difference in the binding energy due to the variation of c_{pair} is about 1 MeV. The minima of the curves are much less defined here than they are in the case of ^{44}S . In fact, the calculation using $c_{pair}=0.50$ appears to have only an oblate minimum. The calculation with $c_{pair}=0.55$ possesses two minima, with the oblate one approximately 200 keV below the prolate one. Due to the lack of structure in the curves, it is difficult to determine the reduction of the deformation at the minima due to the increase in the parameter c_{pair} . The experimental value of the quadrupole deformation of ^{46}Ar is $|\beta|=0.176(17)$ [62], with the sign of the deformation undetermined experimentally. Assuming the deformation to be oblate, the calculated value of $\beta=-0.18$ is in excellent agreement with the data. A nonrelativistic HF calculation furnishes results in reasonable agreement with ours, while its companion RMF+BCS calculation predicts the oblate minimum of the ^{46}Ar energy curve to lie slightly above a spherical ground state [58,59]. The RHB calculation using the Gogny interaction yields a flat energy curve with a barely discernible minimum at $\beta \approx -0.15$ [42].

We have performed calculations of the binding energy as a function of the quadrupole deformation for other $N = 28$ isotones. The binding energies of ^{40}Mg and ^{42}Si are also found to possess both an oblate and a prolate minimum. Just as for ^{44}S , we find that increasing the value of c_{pair} tends to flatten their energy curves and to reduce the magnitude of the deformation at the minima. The calculation using $c_{pair}=0.55$ yields, for ^{42}Si , a sharp oblate minimum at $\beta=-0.32$, about 1 MeV below a shallow prolate minimum at $\beta=0.25$. For ^{40}Mg , the calculation using $c_{pair}=0.55$ yields a fairly shallow prolate minimum at $\beta=0.38$, about 0.5 MeV below a shallow oblate minimum at $\beta=-0.25$. As far as we know, the deformations of these nuclei have not been measured. As mentioned before, a small neutron pairing gap persists in our calculation of the spherical nucleus ^{48}Ca . This gap disappears in the heavier $N=28$ isotones, ^{50}Ti , ^{52}Cr , and ^{54}Fe , which are also spherical, but which possess instead an average proton gap. In Table I, we provide a summary of the ground state energies, deformations, and average gap parameters of the nuclei in the $N = 28$ chain, obtained

with $c_{pair}=0.55$. We note that, except for the lightest nuclei in chain, ^{38}Ne and ^{40}Mg , the calculations are in good agreement with the Audi-Wapstra and Möller-Nix systematics.

In agreement with the other calculations discussed above, we find the even-even nuclei with $A < 48$ in the $N = 28$ isotonic chain to display the characteristics of shape coexistence. The nuclei vary between oblate and prolate ground state deformations and possess both prolate and oblate minima that are very similar in energy. The values we obtain for the ground state deformations are very similar to those of the other calculations. The values obtained for the pairing gaps are different however. The RMF+BCS calculations of Refs. [58] and [59] fixed the gap at either 75 keV or at 500 keV, values which are relatively small for such light nuclei. The RHB calculations of Ref. [42], which are the most similar to our calculations in terms of method, obtained average values of the pairing gap that are about 40% larger than ours, but values for the deformations that are almost identical to ours. If we were to increase the magnitude of the pairing field in our calculations, the resulting deformations would be smaller than those of the RHB (and other) calculations. This discrepancy is an indication of the relativistic effects of the Dirac pairing field that were discussed in the Introduction. There, we suggested that the Dirac structure of the pairing field should result in its being more localized on the nuclear surface and, thus, more effective in limiting the deformation. As the Dirac structure of the pairing field is the principal difference between our calculations and the RHB ones, our results lend support to this argument.

C. Deformed nuclei in the $Z \approx 40$ region

Nuclei in the region of the $Z \approx 40$ subshell closure present interesting variations in deformation as they deviate from the neutron magic number $N = 50$ on either side of the stability line. Studies of their level schemes and lifetimes have shown that the ground-state properties of these nuclei are very sensitive to small changes in the proton and neutron number [63,64].

Strontium isotopes present two regions ($N \approx 38$ and $N \approx 60$) of very strong deformations, as large as $\beta = 0.4$. This behavior can be seen in the E2+ measurements as well as in the isotope shifts. The rapid transition from a spherical shape near the $N=50$ shell closure to a strongly deformed one can be explained by the reinforcement of the shell gaps in the single-particle levels for protons and neutrons [4].

For krypton isotopes, on the other hand, the expected change in shape at $N = 60$, which occurs for most elements in the $Z = 40$ region, does not appear. Instead, the isotope shifts show a pronounced slope change at $N = 50$. The fact that a strongly deformed ground state does not appear at $N = 60$ has been attributed to a reduced proton-neutron interaction at $Z = 36$.

Theoretical studies of these nuclei have been carried out using both relativistic and non-relativistic frameworks. Bonche et al. [54,55] studied these isotopes extensively including triaxial deformations in the non-relativistic Hartree-Fock with a Skyrme SIII force, which resulted in a linear trend for the isotope shifts. They also used the method of generator coordinates for Sr isotopes and predicted a transition from a spherical to a deformed shape. However, the isotope shifts could not be reproduced in any of those calculations.

Many studies using the relativistic mean field approach have been performed in this region. Early calculations employed the parameter set NL1, which has a very large asymmetry energy and does not describe the isotope shifts well [20,21]. In Ref. [22], however, Lalazissis and Sharma successfully described the ground state properties of the Sr and Kr isotopes, by applying the RMF approach with the NLSH parameter set for the mean field Lagrangian and the BCS formalism for the pairing correlations. The deviations of the binding energies from the experimental data were the on order of 0.5% and the deformation parameters β were in good agreement with the β values extracted from B(E2) measurements. It is therefore of interest to perform calculations of the Sr and Kr isotopes using the Dirac-Hartree-Bogoliubov approach in those regions and compare the results with the experimental data.

We begin by studying the dependence of the binding energy on the quadrupole deformation parameter, β , using the method described in the previous section. In Fig. 10, we present the total binding energy as a function of the deformation β of the nucleus ^{100}Sr , for three values of the parameter c_{pair} . The most singular difference between the three curves is the change of the absolute minimum, from a prolate shape in the case of $c_{pair} = 0.51$ to an oblate one for $c_{pair} = 0.54$, remaining oblate for $c_{pair} = 0.58$. The energy difference between the two minima is quite small and the oblate minimum becomes deeper relative to the prolate one as c_{pair} increases. For $c_{pair} = 0.51$, the prolate minimum is 379 keV deeper than the oblate one. For $c_{pair} = 0.54$, the oblate minimum is 17 keV deeper, while for $c_{pair} = 0.58$, it is 823 keV deeper. If we take the oblate solution as the absolute minimum, the value of the deformation parameter agrees well with the experimental value of $\beta = 0.372 \pm 0.008$.

We performed calculations for possible minima of both prolate and oblate shapes of most of the known even nuclei in the Kr and Sr isotopic chains. We found many nuclei for which the two minima have very similar binding energies, an indication of shape coexistence or of a triaxial ground state deformation.

The two-neutron separation energies of the even Kr and Sr isotopes, as functions of the mass number, are shown in Fig. 11, for three values of c_{pair} . To prepare this figure, we have selected the solution, among the multiple minima of each isotope, that has the deepest (absolute) minimum. We compare our results with the Möller-Nix systematics and the Audi-Wapstra compilation. We find the calculations to agree quite well with both of these. As in the previous cases, the calculated two-neutron separation energies are fairly insensitive to the parameter c_{pair} .

In Fig. 12, we display the mean value of the neutron gap parameter $\langle \Delta_n \rangle$ of the even mass Kr and Sr isotopes, as a function of the mass number, for the same three values of c_{pair} . We find the best agreement with the Möller-Nix and Audi-Wapstra values to be given by the calculations using $c_{pair} = 0.58$. The shell closure at $N = 50$ is clearly visible as a zero in the calculated pairing gap of both isotopoic chains.

In Table II, we present the results for the total binding energy and the deformation parameter β obtained in the present calculations, for $c_{pair}=0.58$, together with the experimental data. The value $c_{pair}=0.58$ furnishes the best description of the total binding energies and of the mean value of the neutron pairing gap. The cases in which the difference between two minima is less than 200 keV are marked with a star and the results for the two deformations are presented. In general, the calculated binding energies agree quite well with the experimental values, although the proton-rich isotopes are slightly underbound in the calculations.

Our calculations, with one exception, predict that the non-spherical even nuclei in the two isotopic chains will have an oblate ground state deformation. This contrasts sharply with the Möller-Nix systematics which, with two exceptions, predicts prolate deformations for the ground states of the non-spherical nuclei of the two chains. Such disagreement is not too surprising, given the sensitivity to the interaction parameters of the binding energy versus deformation curve of many of these nuclei. An example of this sensitivity was displayed in Fig. 10, in which the ground state of ^{100}Sr was seen to be prolate for $c_{pair} = 0.51$ but oblate for $c_{pair} = 0.54$ and 0.58 . We note that, of the the five nuclei for which we found a second minimum within 200 keV of the ground state one, the deformation of the second minimum of four of these nuclei is in agreement with the Möller-Nix prediction. Experimentally, large ground state deformations of $\beta \approx 0.44$ have been found in ^{76}Sr , ^{74}Kr , and ^{76}Kr [4]. These values are in agreement with the Möller-Nix ones and with our result for ^{76}Sr . They are not consistent with our results for the Kr isotopes.

The calculated isotope shifts of the even-even Kr and Sr isotopes, with respect to the reference nuclei ^{86}Kr and ^{88}Sr , respectively, are compared to the experimental data in Fig. 13. We display only the results for the deepest energy minimum of each isotope in the figure. In the cases in which a second minimum is close in energy to the deepest one, their isotopic shifts are also very similar. We find the agreement with the data for the neutron rich side to be very good. In addition, the positions of the kink due to the shell effect for the Kr and Sr isotopes are also well reproduced. However, the calculations underestimate the isotope shift on the proton rich side of the stability line.

VII. SUMMARY

We have used an extension of the Gorkov formalism for the description of pairing to develop a Dirac-Hartree-Fock-Bogoliubov approximation to the ground state wave function and energy of finite nuclei. We have applied it to spin-zero proton-proton and neutron-neutron pairing within the Dirac-Hartree-Bogoliubov approximation (we neglected the Fock term). We have retained the full Dirac structure of the pairing field that is permitted by the symmetries of the problem. We find the Dirac pairing structure to be dominated by a scalar term and the zero component of a vector term, as has also been found to be the case for $^1\text{S}_0$ pairing in symmetric nuclear matter.

In our calculations, we use a zero-range approximation to the pairing interaction, which results in a local pairing field. We justified the zero-range approximation by arguing that the effective length for spatial variations of the wavefunctions, in the calculations performed at present, is larger than the range of the nonlocality of the pairing interaction, rendering the effects of the nonlocality close to negligible.

We studied the effects of the Dirac pairing field on the properties of the even-even nuclei of the isotopic chains of Ca, Ni and Sn (spherical) and Kr and Sr (deformed), as well as the $N=28$ isotonic chain. We first studied the isotopic chains of the spherical nuclei in order to determine the sensitivity of various nuclear observables to the interaction in the pairing channel. We found the two-neutron separation energies, root-mean-square radii and isotopic shifts of the spherical nuclei to be fairly independent of the strength of the pairing interaction. The binding energy, on the contrary, is quite sensitive to the pairing interaction

strength (at least when the pairing is not identically zero due to a shell closure). Quite obviously, the average pairing gap also displays a strong dependence on the strength of the pairing interaction. We observed that an adequate choice of this strength simultaneously yields reasonable values for the binding energy, near the stability line, and rough agreement between the average pairing gap and the experimental gap, defined in terms of even-odd mass differences. Far from the stability line, our calculated binding energies showed increasing discrepancies with the experimental data, suggesting that the NL3 parameter set might require further adjustment, at least when used in a DHB formalism. All in all, however, our results show good agreement with the data and with previous calculations.

To study the deformed Kr and Sr nuclei and the deformed nuclei of the $N=28$ isotonic chain, we performed a sequence of constrained Dirac-Hartree-Bogoliubov calculations, as a function of the quadrupole deformation β , for each of the nuclei in question. Each sequence of calculations provided us with a curve of binding energy versus deformation that permitted the localization of the equilibrium configurations of the nucleus. Most of the nuclei in these three chains present both a prolate and an oblate minimum (and, at times, a slight spherical minimum as well). In agreement with other calculations, we found nuclei in each of the chains for which the energies of the oblate and prolate minima were very similar, raising the possibility of shape coexistence or triaxial ground state deformations. For the most part, our results present reasonable agreement with the data and with previous calculations. We did, however, observe a discrepancy between our average pairing gaps and those of the RHB calculations of Ref. [42], which we took as an indication of the relativistic suppression of the pairing field due to its Dirac structure. Our DHB calculations furnished quadrupole deformations similar to the RHB ones for average values of the pairing gap that are about 30% smaller than theirs.

Based on the nuclei we have studied here, we conclude that the DHB approximation can provide a description of the binding energies, rms radii and ground state deformations of finite nuclei that is at least as good as that provided by the nonrelativistic HFB approximation or by the RHB approximation. Our claim that the DHB approximation can provide a more reliable description than the others, however, has not been demonstrated here. This will require further study of the parameters that enter the pairing interaction, in order to better fix their values.

In the future, we plan to extend our calculations to a larger set of isotopic chains and to analyze in detail their proton- and neutron-rich tails, in order to obtain a set of parameters that describes these better. We plan to extend our calculations to odd nuclei by including a blocking term. As the blocking term varies, along with the other states, during the search for the Dirac-Hartree-Bogoliubov stationary point, this does not seem to be a trivial task. In order to facilitate it, we plan to first develop an extended BCS approximation, based on the self-consistent Hartree eigenstates of the mean field in conjunction with the relativistic pairing field. Such an approximation could also serve as a faster first stage to the Dirac-Hartree-Bogoliubov calculations, which are quite time-consuming at the present. Eventually, we also intend to include the nonlocality of the pairing interaction, in order to use more realistic interactions containing the relatively long-range effects of pion exchange.

ACKNOWLEDGMENTS

The authors would like to thank P. Ring for providing them with an early version of the Munich deformed relativistic Hartree code [65], which served as the starting point for the code used for the calculations described here. The authors acknowledges partial support from FAPESP (Fundação de Amparo à Pesquisa do Estado de São Paulo). B.V.C. acknowledges partial support from the CNPq (Conselho Nacional de Pesquisa e Desenvolvimento).

REFERENCES

- [1] I. Tanihata, H. Hamagaki, O. Hashimoto, Y. Shida, N. Yoshikawa, K. Sugimoto, O. Yamakawa, T. Kobayashi and N. Takahashi, Phys. Rev. Lett. **55**, 2676 (1985).
- [2] I. Tanihata, D. Hirata, T. Kobayashi, S. Shimoura, K. Sugimoto and H. Toki, Phys. Lett. **B289**, 261 (1992).
- [3] T. Suzuki, H. Geissel, O. Bochkarev, L. Chulkov, M. Golovkov, D. Hirata, H. Irnich, Z. Janas, H. Keller, T. Kobayashi, G. Kraus, G. Münzenberg, S. Neumaier, F. Nickel, A. Ozawa, A. Piechaczek, E. Roeckl, W. Schwab, K. Sümmerer, K. Yoshida, I. Tanihata, Phys. Rev. Lett. **75**, 3241 (1995).
- [4] J.H. Hamilton, Treatise on Heavy Ion Science, **8**, ed. D. A. Bromley (Plenum, New York, 1989) p.3.
- [5] I. Tanihata, Progress in Particle and Nuclear Physics **35**, 505 (1995).
- [6] Proceedings of the Fourth International Conference on Radioactive Nuclear Beams, Ohmiya, Japan, 1996, Nucl. Phys. **A616** (1997).
- [7] B.D.Serot and J.D.Walecka, Adv. Nucl. Phys. **16**, 1 (1986).
- [8] P.G. Reinhard, Rep. Prog. Phys. **52**, 439 (1989).
- [9] B. D. Serot, Rep. Prog. Phys. **55**, 1855 (1992).
- [10] R. Brockmann and R. Machleidt, Phys. Rev. C **42**, 1965 (1990).
- [11] L.D. Miller and A.E.S. Green, Phys. Rev. C **5**, 241 (1972).
- [12] R. Brockmann, Phys. Rev. C **18**, 1510 (1978).
- [13] R. Brockmann and W. Weise, Nucl. Phys. **A355**, 365 (1981).
- [14] C.J. Horowitz and B.D. Serot, Nucl. Phys. **A368**, 503 (1981).
- [15] C.E. Price and G.E. Walker, Phys. Rev. C **36**, 355 (1987).
- [16] A. Bouyssy, J.F. Mathiot, N.V. Giai and S. Marcos, Phys. Rev. C **36**, 380 (1987).
- [17] Y.K. Gambhir, P. Ring and A. Thimet, Ann. Phys.(NY), **198**, 132 (1990).
- [18] D. Hirata, H. Toki, T. Watabe, I. Tanihata and B. V. Carlson, Phys. Rev. C **44**, 1467 (1991).
- [19] M.M. Sharma and P. Ring, Phys. Rev. C **46**, 1715 (1992).
- [20] D. Hirata, H. Toki, I. Tanihata and P. Ring, Phys. Lett. B **314**, 168 (1993).
- [21] J.A. Sheikh and P. Ring, Phys. Rev. C **47**, R1850 (1993).
- [22] G.A. Lalazissis and M.M. Sharma, Nucl. Phys. **A586**, 201 (1995).
- [23] P. Ring, Prog. Part. Nucl. Phys. **37**, 193 (1996).
- [24] K. Pomorski, P. Ring, G.A. Lalazissis, A. Baran, Z. Lojewski, B. Nerlo-Pomorska and M. Warda, Nucl. Phys. **A624**, 349 (1997).
- [25] D. Hirata, K. Sumiyoshi, I. Tanihata, Y. Sugahara, T. Tachibana, and H. Toki Nucl. Phys. **A616**, 438c (1997).
- [26] G.A. Lalazissis, A.R. Farhan, and M.M. Sharma, Nucl. Phys. **A628**, 221 (1998).
- [27] D. Bailin and A. Love, Phys. Rep. **107C**, 325, (1984).
- [28] H. Kucharek and P. Ring, Z. Phys. A **339**, 23 (1991).
- [29] F.B. Guimarães, B.V. Carlson and T. Frederico, Phys. Rev. C **54** 2385 (1996).
- [30] F. Matera, G. Fabbri and A. Dellafore, Phys. Rev. C **56**, 2385 (1997).
- [31] B.V. Carlson, T. Frederico and F.B. Guimarães, Phys. Rev. C **56** 3097 (1997).
- [32] Ø. Elgarøy , L. Engvik, M. Hjorth-Jensen and E. Osnes, Phys. Rev. C **57**, 1069 (1998).
- [33] J. Meng and P. Ring, Phys. Rev. Lett. **77**, 3963 (1996).

- [34] T. Gonzalez-Llarena, J.L. Egido, G.A. Lalazissis, and P. Ring, Phys. Lett. B **379**, 13 (1996).
- [35] W. Pöschl, D. Vretenar, G.A. Lalazissis, and P. Ring, Phys. Rev. Lett. **79**, 3841 (1997).
- [36] G.A. Lalazissis, D. Vretenar, W. Pöschl, and P. Ring, Nucl. Phys. **A632**, 363 (1998).
- [37] G.A. Lalazissis, D. Vretenar, W. Pöschl, and P. Ring, Phys. Lett. B **418**, 7 (1998).
- [38] J. Meng, Phys. Rev. C **57**, 1229 (1998).
- [39] D. Vretenar, W. Pöschl, G.A. Lalazissis, and P. Ring, Phys. Rev. C **57**, R1060 (1998).
- [40] G.A. Lalazissis, D. Vretenar, and P. Ring, Phys. Rev. C **57**, 2294 (1998).
- [41] D. Vretenar, G.A. Lalazissis, and P. Ring, Phys. Rev. C **57**, 3071 (1998).
- [42] G.A. Lalazissis, D. Vretenar, P. Ring, M. Stoitsov, and L. Robledo, Phys. Rev. C, **60**, 014310 (1999).
- [43] L.N. Cooper, Phys. Rev. **104**, 1189 (1956).
- [44] L.P. Gorkov, Sov. Phys. JETP **34(7)**, 505 (1958).
- [45] C. Itzykson and J.B. Zuber, *Quantum Field Theory*, McGraw-Hill, New York, 1980.
- [46] M. Baldo, U. Lombardo, and P. Schuck, Phys. Rev. C **52**, 975 (1995).
- [47] V. A. Khodel, V. V. Khodel and J. W. Clark, Nucl. Phys. **A598**, 390 (1996).
- [48] Ø. Elgarøy, L. Engvik, M. Hjorth-Jensen and E. Osnes, Nucl. Phys. **A604**, 466 (1996).
- [49] D. Vautherin, Phys. Rev. C **25**, 571 (1980).
- [50] M. Abramowitz and I.A. Stegun, *Handbook of Mathematical Functions*, Dover, New York, 1970.
- [51] G.A. Lalazissis, J. König, and P. Ring, Phys. Rev. C **55**, 540 (1997).
- [52] J. Dobaczewski, W. Nazarewicz, T.R. Werner, J.F. Berger, C.R. Chinn, and J. Dechargé, Phys. Rev. C **53**, 2809 (1996).
- [53] M.M. Sharma, M.A. Nagarajan, and P. Ring, Phys. Lett. B **312**, 377 (1993).
- [54] P. Bonche, H. Flocard, P.H. Heenen, S.J. Krieger and M.S. Weiss, Nucl. Phys. **A 443**, 39 (1985).
- [55] P. Bonche, J. Dobaczewski and H. Flocard, Nucl. Phys. **A530**, 149 (1991).
- [56] P. Möller, J.R. Nix, W.D. Myers, and W.J. Swiatecki, At. Data Nucl. Data Tables **61**, 127 (1995).
- [57] G. Audi and A.H. Wapstra, Nucl. Phys. **A 595**, 409 (1995).
- [58] T.R. Werner, J.A. Sheikh, W. Nazarewicz, M.R. Strayer, A.S. Umar, and M. Misu, Phys. Lett. **B335**, 259 (1994).
- [59] T.R. Werner, J.A. Sheikh, M. Misu, W. Nazarewicz, J. Rikowska, K. Heeger, A.S. Umar, and M.R. Strayer, Nucl. Phys. **A597**, 327 (1996).
- [60] T. Glasmacher et al. Phys. Lett. **B395**, 163 (1997).
- [61] T. Glasmacher, Nucl. Phys. **A630**, 278c (1998).
- [62] H. Scheit et al., Phys. Rev. Lett. **77**, 3967 (1996).
- [63] F. Buchinger, E.B. Ramsay, E. Arnold, W. Neu, R. Neugart, K. Wendt, R.E. Silverans, P. Lievens, L. Vermeeren, D. Berdichevsky, R. Fleming, D.W.L. Sprung, G. Ulm, Phys. Rev. C **41**, 2883 (1990).
- [64] M. Keim, E. Arnold, W. Borchers, U. Georg, A. Klein, R. Neugart, L. Vermeeren, R.E. Silverans, P. Lievens, Nucl. Phys. **A 586**, 219 (1995).
- [65] W. Pöschl, D. Vretenar, P. Ring, Comput. Phys. Commun. **103**, 217 (1997).

APPENDIX A: TIME-REVERSED PAIRS OF STATES

We begin by writing the complex conjugate of Eq. (25) as

$$\int d^3y \begin{pmatrix} \gamma_0((\varepsilon + \mu)\delta(\vec{x} - \vec{y}) - Bh^*(\vec{x}, \vec{y})B^\dagger) & B\Delta^*(\vec{x}, \vec{y})B^\dagger \\ B\bar{\Delta}^*(\vec{x}, \vec{y})B^\dagger & ((\varepsilon - \mu)\delta(\vec{x} - \vec{y}) + Bh_T^*(\vec{x}, \vec{y})B^\dagger)\gamma_0 \end{pmatrix} \begin{pmatrix} BU^*(\vec{y}) \\ BV^*(\vec{y}) \end{pmatrix} = 0, \quad (\text{A1})$$

where $B = \gamma_5 C$ is the Dirac matrix part of the time-reversal operator. Analyzing the Hamiltonian term, we see that

$$\begin{aligned} Bh^*(\vec{x}, \vec{y})B^\dagger &= B(i\vec{\alpha}^* \cdot \vec{\nabla} + \beta^* M)B^\dagger \delta(\vec{x} - \vec{y}) + B\beta^* \Sigma^*(\vec{x}, \vec{y})B^\dagger \\ &= (-i\vec{\alpha} \cdot \vec{\nabla} + \beta M)\delta(\vec{x} - \vec{y}) + B\beta^* \Sigma^*(\vec{x}, \vec{y})B^\dagger. \end{aligned} \quad (\text{A2})$$

The self-energy term, in turn, can be put into the form

$$\begin{aligned} B\beta^* \Sigma(\vec{x}, \vec{y})B^\dagger &= \delta(\vec{x} - \vec{y}) \sum_j B\gamma_0^* \Gamma_{j\alpha}^*(\vec{x})B^\dagger \int d^3z D_j^{\alpha\beta}(\vec{x} - \vec{z}) \sum_{\varepsilon_\gamma < 0} U_\gamma^T(\vec{z})B^\dagger B\gamma_0^* \Gamma_{j\beta}^*(\vec{z})B^\dagger BU_\gamma^*(\vec{z})B^\dagger \\ &\quad - \sum_j B\gamma_0^* \Gamma_{j\alpha}^*(\vec{x})B^\dagger D^{\alpha\beta}(\vec{x} - \vec{y}) \sum_{\varepsilon_\gamma < 0} BU_\gamma^*(\vec{x})U_\gamma^T(\vec{y})B^\dagger B\gamma_0^* \Gamma_{j\beta}^*(\vec{y})B^\dagger. \end{aligned} \quad (\text{A3})$$

If we now look closely at the vertex functions we are considering here, we find

for the σ meson: $B\gamma_0^* 1 B^\dagger \dots B\gamma_0^* 1 B^\dagger = \gamma_0 1 \dots \gamma_0 1$,

for the ω meson: $B\gamma_0^* \gamma_\mu^* B^\dagger g^{\mu\nu} \dots B\gamma_0^* \gamma_\nu^* B^\dagger = \gamma_0 \gamma_\mu g^{\mu\nu} \dots \gamma_0 \gamma_\nu$,

for the ρ meson: $B\gamma_0^* \gamma_\mu^* \tau_i^* B^\dagger g^{\mu\nu} \delta^{ij} \dots B\gamma_0^* \gamma_\nu^* \tau_j^* B^\dagger = \gamma_0 \gamma_\mu \tau_i g^{\mu\nu} \delta^{ij} \dots \gamma_0 \gamma_\nu \tau_j$,

for the photon: $B \frac{(1+\tau_3^*)}{2} \gamma_0^* \gamma_\mu^* B^\dagger g^{\mu\nu} \dots B \frac{(1+\tau_3^*)}{2} \gamma_0^* \gamma_\nu^* B^\dagger = \frac{(1+\tau_3)}{2} \gamma_0 \gamma_\mu g^{\mu\nu} \dots \frac{(1+\tau_3)}{2} \gamma_0 \gamma_\nu$. In short, the products of the pairs of vertices remain unchanged by the transformation. We thus have for the transformed self energy,

$$\begin{aligned} B\beta^* \Sigma^*(\vec{x}, \vec{y})B^\dagger &= \delta(\vec{x} - \vec{y}) \sum_j \gamma_0 \Gamma_{j\alpha}(\vec{x}) \int d^3z D_j^{\alpha\beta}(\vec{x} - \vec{z}) \left(\sum_{\varepsilon_\gamma < 0} U_\gamma^T(\vec{z})B^\dagger \gamma_0 \Gamma_{j\beta}(\vec{z})BU_\gamma^*(\vec{z}) \right) \\ &\quad - \sum_j \gamma_0 \Gamma_{j\alpha}(\vec{x}) D^{\alpha\beta}(\vec{x} - \vec{y}) \left(\sum_{\varepsilon_\gamma < 0} BU_\gamma^*(\vec{x})U_\gamma^T(\vec{y})B^\dagger \gamma_0 \right) \Gamma_{j\beta}(\vec{y}), \end{aligned} \quad (\text{A4})$$

in which the only differences from the original expression for the self energy are the propagator contributions, written in terms of the solutions of the Dirac-Gorkov equation, that enter the expression.

We can perform the same analysis on the pairing term, for which we find a similar result,

$$B\Delta^*(\vec{x}, \vec{y})B^\dagger = - \sum_j \Gamma_{j\alpha}(\vec{x}) D_j^{\alpha\beta}(\vec{x} - \vec{y}) \left(\sum_{\varepsilon_\gamma < 0} BU_\gamma^*(\vec{x})V_\gamma^T(\vec{y})B^\dagger \gamma_0 \right) A\Gamma_{j\beta}^T(\vec{y})A^\dagger, \quad (\text{A5})$$

in which the only difference between the original expression and the transformed one is again the propagator's contribution to the expression. Analyses of the other terms, $Bh_T^*(\vec{x}, \vec{y})B^\dagger$ and $B\bar{\Delta}^*(\vec{x}, \vec{y})B^\dagger$, yield similar results.

We can thus show that the transformed wave vector $\begin{pmatrix} BU^*(\vec{x}) \\ BV^*(\vec{x}) \end{pmatrix}$ satisfies a similar equation

$$\int d^3y \begin{pmatrix} \gamma_0((\varepsilon + \mu)\delta(\vec{x} - \vec{y}) - h(\vec{x}, \vec{y})) & \Delta(\vec{x}, \vec{y}) \\ \bar{\Delta}(\vec{x}, \vec{y}) & ((\varepsilon - \mu)\delta(\vec{x} - \vec{y}) + h_T(\vec{x}, \vec{y}))\gamma_0 \end{pmatrix} \begin{pmatrix} BU^*(\vec{y}) \\ BV^*(\vec{y}) \end{pmatrix} = 0, \quad (\text{A6})$$

to that satisfied by the wavevector $\begin{pmatrix} U(\vec{x}) \\ V(\vec{x}) \end{pmatrix}$. Each is a solution of an equation with the same energy eigenvalue but with orbital quantum numbers and mean fields that have the time-reversed Dirac structure of the other. If each member of these pairs of states possessing time-reversed Dirac structure are equally occupied, the sums over states that enter into the definition of the self-energy and pairing fields will be invariant under the transformation that temporally inverts the Dirac structure. That is, we then have that

$$\sum_{\varepsilon_\gamma < 0} U_\gamma(\vec{x})U_\gamma^\dagger(\vec{y}) = \sum_{\varepsilon_\gamma < 0} BU_\gamma^*(\vec{x})U_\gamma^T(\vec{y})B^\dagger \quad (\text{A7})$$

and

$$\sum_{\varepsilon_\gamma < 0} U_\gamma(\vec{x})V_\gamma^\dagger(\vec{y}) = \sum_{\varepsilon_\gamma < 0} BU_\gamma^*(\vec{x})V_\gamma^T(\vec{y})B^\dagger. \quad (\text{A8})$$

In this case, both of the wavevectors $\begin{pmatrix} U(\vec{x}) \\ V(\vec{x}) \end{pmatrix}$ and $\begin{pmatrix} BU^*(\vec{x}) \\ BV^*(\vec{x}) \end{pmatrix}$ satisfy the same Dirac-Gorkov equation with the same energy eigenvalue. Then either both or neither of them will enter the propagator's contributions to the self-consistency equations and these contributions will indeed be invariant under time-inversion of their Dirac structure. We assume this to be the case.

Table 1

	B.E.			β		$\langle \Delta_n \rangle$	$\langle \Delta_p \rangle$
	DHB	A-W	M-N	M-N	DHB	DHB	DHB
³⁸ Ne	-225.19		-214.03	-0.29	0.28	2.21	1.19
⁴⁰ Mg	-272.48		-268.04	-0.29	0.39	1.86	0.00
⁴² Si	-315.53	-313.04	-315.16	-0.32	-0.32	1.24	0.00
⁴⁴ S	-352.78	-353.49	-351.99	0.00	0.28	1.42	0.00
⁴⁶ Ar	-385.58	-386.91	-386.18	0.00	-0.18	1.19	0.00
⁴⁸ Ca	-415.05	-415.98	-415.56	0.00	0.00	0.84	0.00
⁵⁰ Ti	-436.99	-437.77	-438.65	0.00	0.00	0.00	1.55
⁵² Cr	-455.58	-456.34	-457.27	0.00	0.00	0.00	1.52
⁵⁴ Fe	-470.69	-471.75	-472.58	0.00	0.00	0.00	1.06
⁵⁶ Ni	-482.67	-483.98	-484.48	0.00	0.00	0.00	0.00

Table 2

Kr					Sr				
A	B.E.		β		A	B.E.		β	
	DHB	Exp.	DHB	M - N		DHB	Exp.	DHB	M - N
72	-604.25	-607.11	-0.32	-0.35	76	-635.48	-638.08	0.49	0.42
74	-629.51	-631.28	-0.30	0.40	78	-661.70*	-663.01	-0.17 (0.47)	0.42
76	-653.51*	-654.23	-0.20 (0.00)	0.40	80	-686.41	-686.28	0.00	0.05
78	-675.86	-675.55	0.00	-0.23	82	-709.43	-708.13	0.00	0.05
80	-696.75	-695.43	0.00	0.06	84	-730.94	-728.90	0.00	0.05
82	-716.19	-714.27	0.00	0.07	86	-750.99	-748.92	0.00	0.05
84	-734.19	-732.26	0.00	0.06	88	-769.17	-768.46	0.00	0.05
86	-750.29	-749.23	0.00	0.05	90	-782.74	-782.63	0.00	0.05
88	-762.20	-761.80	0.00	0.06	92	-795.15*	-795.75	-0.12 (0.10)	0.08
90	-773.08*	-773.21	-0.14 (0.14)	0.16	94	-807.22	-807.81	-0.18	0.26
92	-783.63*	-783.22	-0.27 (0.20)	0.23	96	-818.67	-818.10	-0.23	0.34
94	-793.59	-791.76	-0.29	0.31	98	-829.36	-827.87	-0.26	0.36
96	-802.77	-799.95	-0.16	0.34	100	-839.29	-837.62	-0.25	0.37

FIGURES

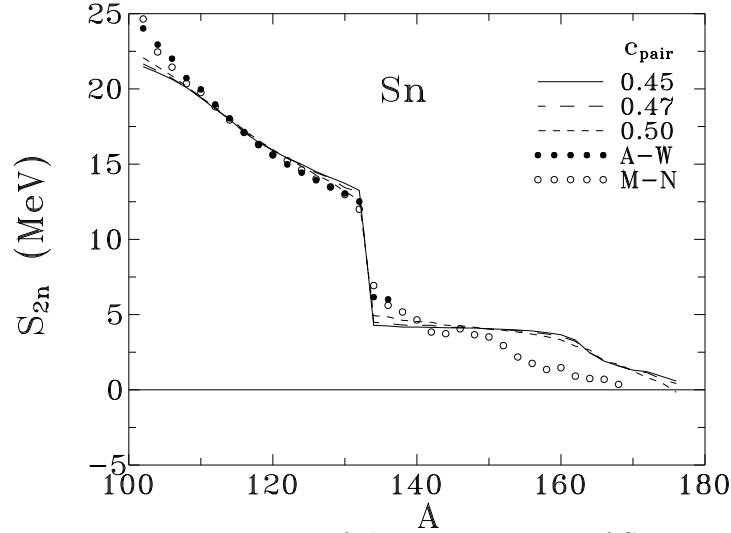


FIG. 1. Two-neutron separation energy of the even isotopes of Sn, as a function of the mass number A , for three values of the parameter c_{pair} . The values obtained from the compilation of experimental masses of Audi and Wapstra [57] (solid circles) and the Möller-Nix systematics [56] (open circles) are also shown.

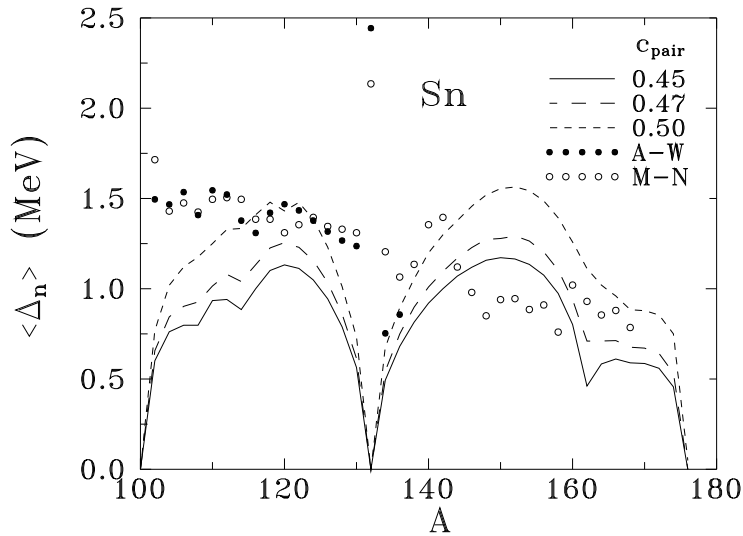


FIG. 2. Mean value of the neutron gap parameter of the even isotopes of Sn, as a function of the mass number A , for three values of the parameter c_{pair} (lines). The odd-even mass differences obtained from the compilation of experimental masses of Audi and Wapstra [57] (solid circles) and from the Möller-Nix systematics [56] (open circles) are also plotted.

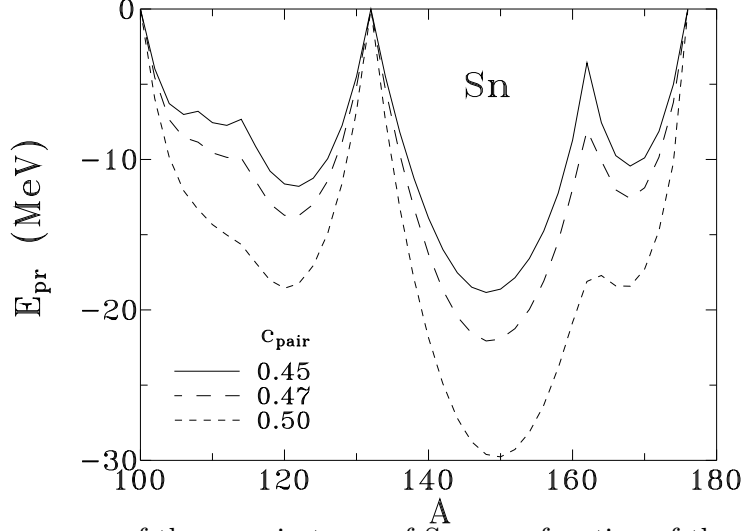


FIG. 3. Pairing energy of the even isotopes of Sn, as a function of the mass number A , for three values of the parameter c_{pair} .

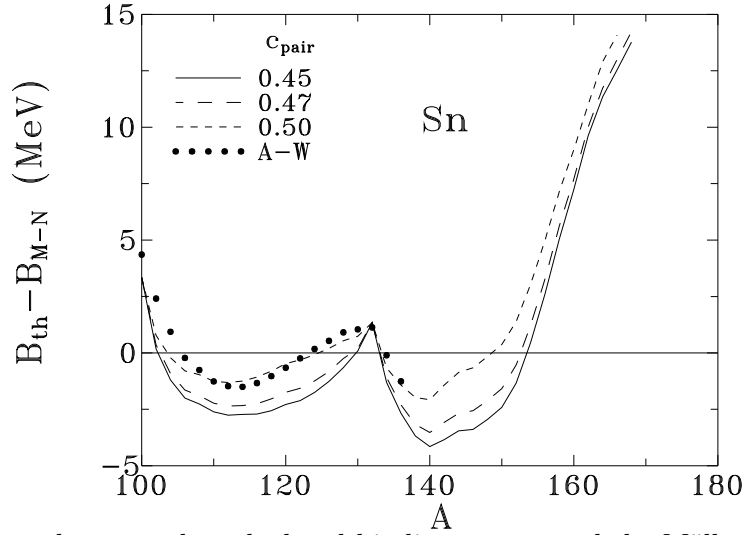


FIG. 4. Difference between the calculated binding energy and the Möller-Nix binding energy [56] for the even isotopes of Sn, as a function of the mass number A , for three values of the parameter c_{pair} (lines). The difference between the calculated binding energy and the Audi-Wapstra experimental binding energy [57], for $c_{pair}=0.500$, is also plotted (circles).

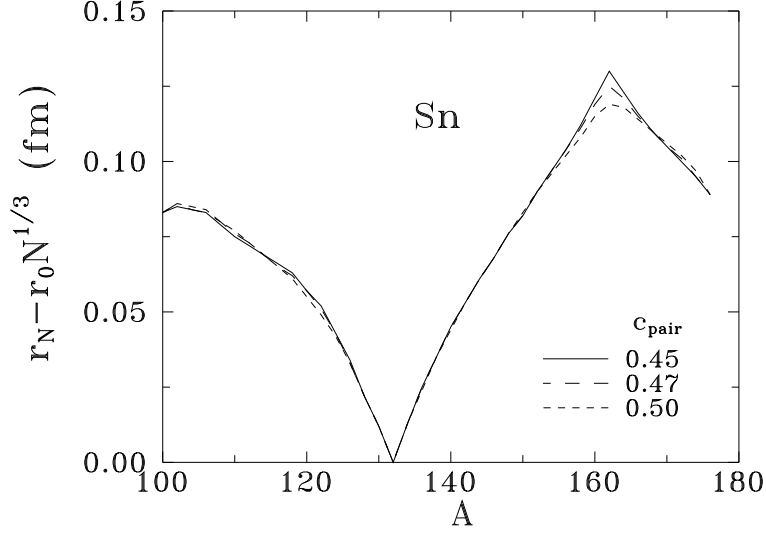


FIG. 5. Deviation of the root mean square neutron radius from the systematic value $r_0 N^{1/3}$, for the even isotopes of Sn, as a function of the mass number A , for three values of the parameter c_{pair} . The reduced radius, r_0 , was adjusted to the root mean square neutron radius of ^{132}Sn .

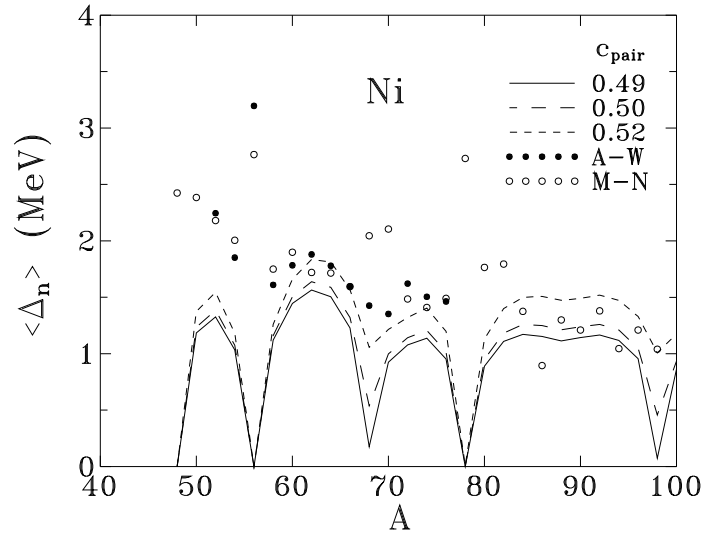


FIG. 6. Mean value of the neutron gap parameter of the even isotopes of Ni, as a function of the mass number A , for three values of the parameter c_{pair} (lines). The odd-even mass differences obtained from the compilation of experimental masses of Audi and Wapstra [57] (solid circles) and from the Möller-Nix systematics [56] (open circles) are also plotted.

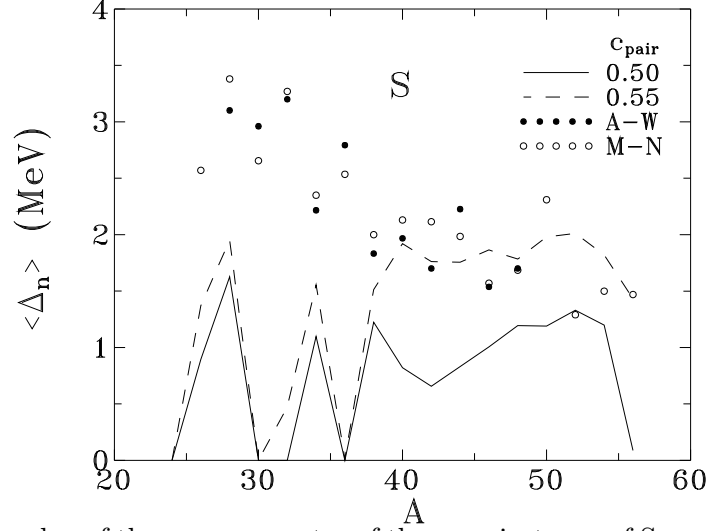


FIG. 7. Average value of the gap parameter of the even isotopes of S, as a function of the mass number A , for two values of the parameter c_{pair} (lines). The odd-even mass differences obtained from the compilation of experimental masses of Audi and Wapstra [57] (solid circles) and from the Möller-Nix systematics [56] (open circles) are also plotted.

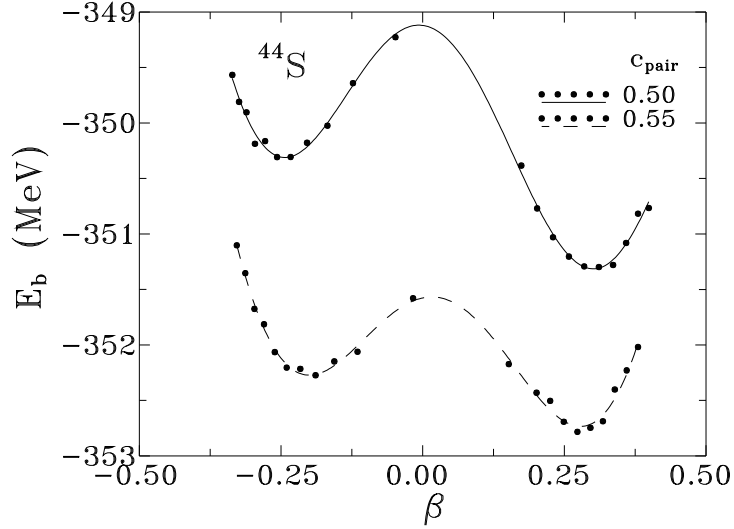


FIG. 8. Binding energy of ^{44}S , as a function of the quadrupole deformation β , for two values of the parameter c_{pair} .

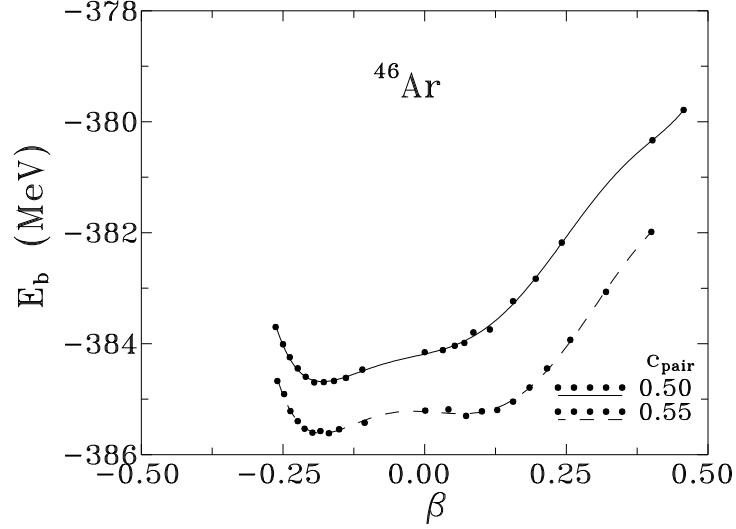


FIG. 9. Binding energy of ^{46}Ar , as a function of the quadrupole deformation β , for two values of the parameter c_{pair} .

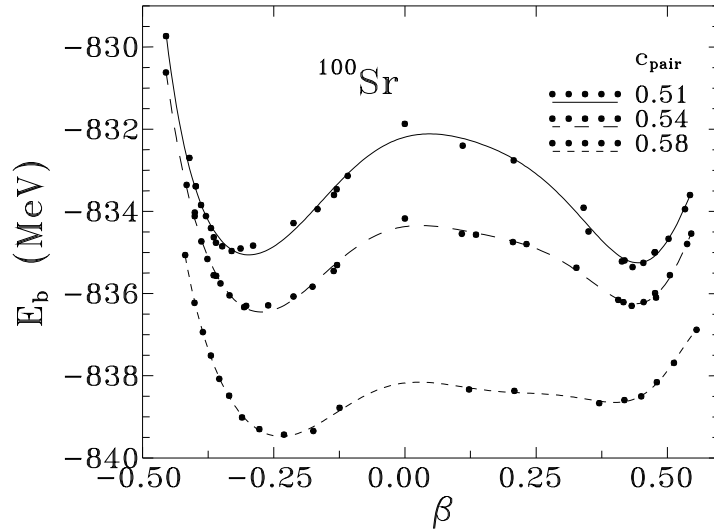


FIG. 10. Binding energy of ^{100}Sr , as a function of the quadrupole deformation β , for three values of the parameter c_{pair} .

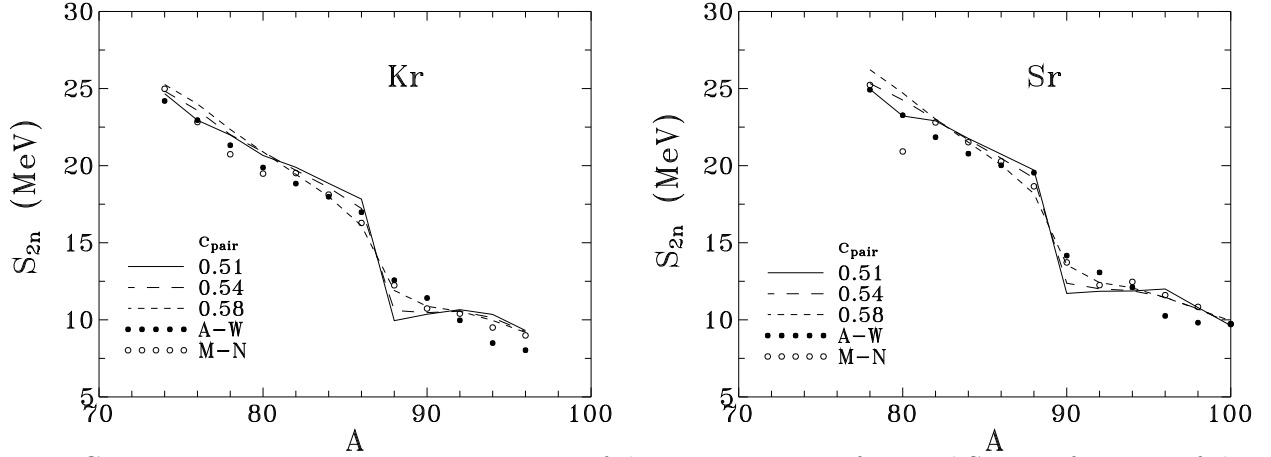


FIG. 11. Two neutron separation energy of the even isotopes of Kr and Sr, as a function of the mass number A , for three values of the parameter c_{pair} . The values obtained from the compilation of experimental masses of Audi and Wapstra [57] (solid circles) and the Möller-Nix systematics [56] (open circles) are also shown.

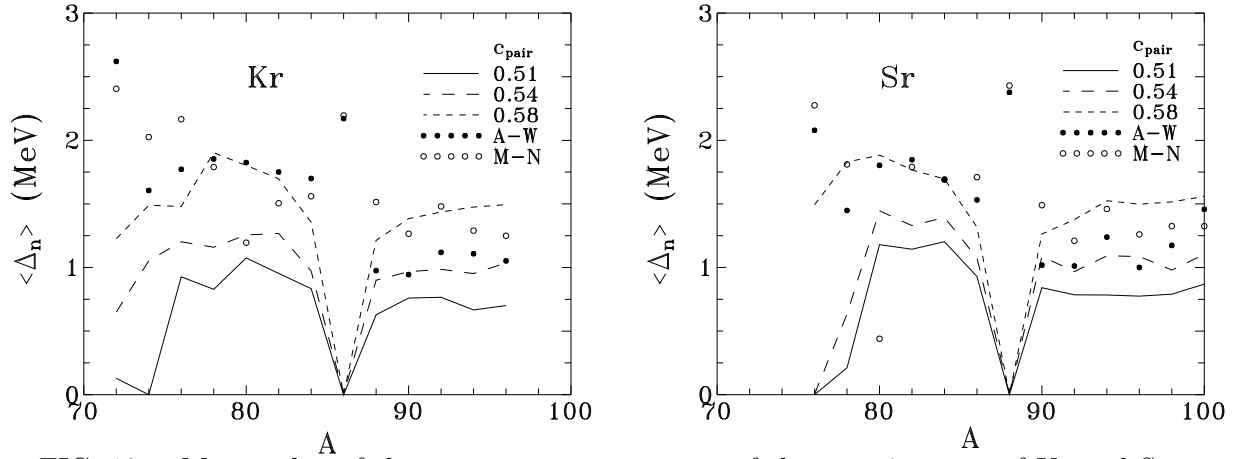


FIG. 12. Mean value of the neutron gap parameter of the even isotopes of Kr and Sr, as a function of the mass number A , for three values of the parameter c_{pair} (lines). The odd-even mass differences obtained from the compilation of experimental masses of Audi and Wapstra [57] (solid circles) and from the Möller-Nix systematics [56] (open circles) are also plotted.

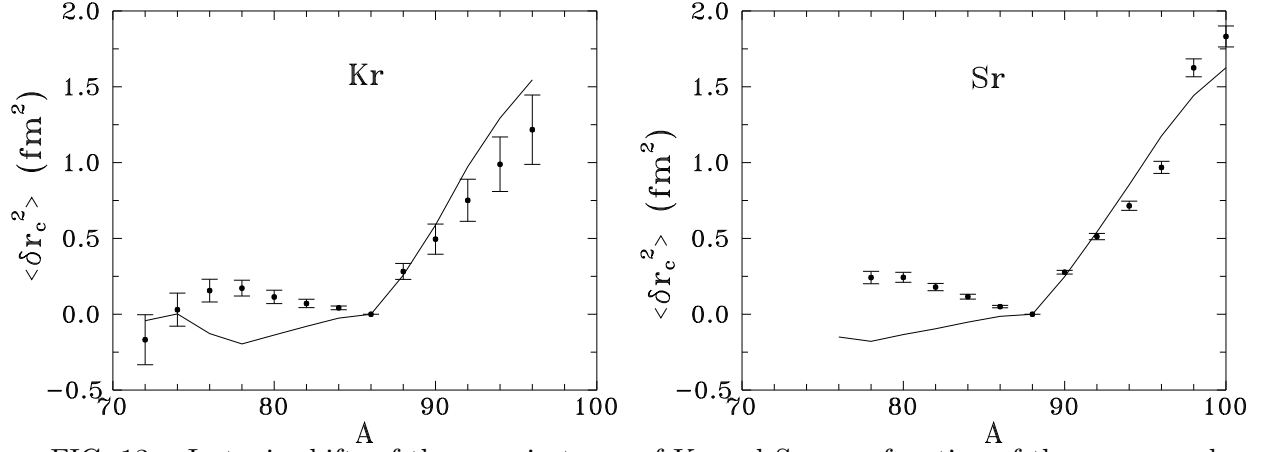


FIG. 13. Isotopic shifts of the even isotopes of Kr and Sr, as a function of the mass number A , for $c_{pair}=0.58$ (lines). The experimental values are displayed as points with error bars.